Optimized Waveforms for 5G–6G Communication With Sensing: Theory, Simulations and Experiments

Sahan Damith Liyanaarachchi, *Graduate Student Member, IEEE*, Taneli Riihonen, *Member, IEEE*, Carlos Baquero Barneto, *Graduate Student Member, IEEE*, and Mikko Valkama, *Senior Member, IEEE*

***Abstract*— Joint communication and sensing (JCAS) is an emerging technology for managing efficiently the scarce radio frequency (RF) spectrum, and is expected to be a key ingredient in beyond fifth-generation (5G) networks. We consider a JCAS system, where the full-duplex radar transceiver and the communication transmitter are the same device, and pursue orthogonal frequency-division multiplexing (OFDM) waveform optimization by jointly minimizing the lower bounds of delay and Doppler estimation. This is attained by filling the empty subcarriers within the OFDM frame with optimized samples while reallocating a proportion of the communication subcarriers' power, which essentially controls the fairness between the two functionalities. Both communication and filled *radar subcarriers* are used for radar processing. The optimized sample values are found analytically, and a computationally feasible algorithm is presented for this task. We also address how the peak-to-average power ratio of the waveform can be controlled and minimized along the optimization process. The results are then numerically evaluated in 5G New Radio (NR) network context, which indicate a trade-off between the minimization of the lower bounds. The main-lobe width and the peak side-lobe level (PSL) of the range and velocity profiles of the radar image are also analyzed. An inverse relation between the lower bounds and the PSLs is observed, while the main-lobe width can be minimized simultaneously. The trade-off between communication and sensing is investigated, which indicates that the lower bounds can be improved at the cost of the communication capacity. Moreover, over-the-air RF measurements are carried out with unoptimized and optimized 5G NR waveforms at the 28 GHz mm-wave band, to validate the range profile's PSL improvement in an outdoor mapping scenario, depicting considerable performance gain.**

***Index Terms*— 5G NR, 6G, JCAS, joint communication and sensing, joint radar-communication, LTE, multi-functional RF systems, OFDM, radar, RF convergence.**

Manuscript received December 24, 2020; revised April 21, 2021 and June 16, 2021; accepted June 17, 2021. Date of publication June 30, 2021; date of current version December 10, 2021. This work was supported in part by the Academy of Finland under Grant 315858, Grant 319994, Grant 328214, and Grant 341489; in part by Nokia Bell Labs; in part by the Doctoral School of Tampere University; and in part by the Finnish Funding Agency for Innovation through the "RF Convergence" project. The associate editor coordinating the review of this article and approving it for publication was W. Zhang. *(Corresponding author: Sahan Damith Liyanaarachchi.)*

The authors are with the Unit of Electrical Engineering, Tampere University, 33720 Tampere, Finland (e-mail: sahan.liyanaarachchi@tuni.fi; taneli.riihonen@tuni.fi; carlos.baquerobarneto@tuni.fi; mikko.valkama@tuni.fi).

Color versions of one or more figures in this article are available at https://doi.org/10.1109/TWC.2021.3091806.

Digital Object Identifier 10.1109/TWC.2021.3091806

I. Introduction

COMMUNICATION and radar/sensing systems have functioned separately and independently from each other in the past. The former have since then developed considerably, e.g., in the form of fifth-generation (5G) mobile communication networks [1] while there are already emerging research efforts towards the sixth-generation (6G) systems. With further advances in, e.g., electronics and signal processing techniques, the communication and sensing systems can be potentially co-located [2]. Due to similar operating frequencies in both systems, their spectra will coincide [3], resulting in mutual interference and potential performance degradation [4]–[6]. The major reason for this is that the radar systems operate at fixed frequencies, which cause the available dedicated spectrum for communication systems to become a scarce resource [7]. Radio frequency (RF) convergence is the umbrella of solutions under which the most novel methodologies exist to combat this challenge [8], where the scarce spectrum is utilized to jointly improve the sensing and communication functionalities. The use of similar hardware solutions in the two systems, such as phased-arrays, has also complemented RF convergence. Thus, a joint communication and sensing (JCAS) system can be pursued [2], [9], with shared waveform and hardware, and minimal performance degradation for both functionalities. For further information, prominent surveys on the topic can be found in [2], [8]–[15] to name but a few.

There are various application contexts for JCAS research, such as cellular networks [16], [17], joint vehicular-communication systems [18]–[20] and indoor mapping [21]. In such applications, the transmit (TX) antennas for the two subsystems are considered to be the same, allowing a single joint waveform to be used for both subsystems' tasks. Since the resources are shared, this will create an inherent trade-off between the two [22]. In designing and optimizing the joint waveform, performance metrics of both subsystems are thus to be taken into consideration. To this end, constrained optimization can be pursued to maximize or minimize the chosen metric of one subsystem, while the other subsystem's metric is properly constrained [23]. For communications, the primary metric is the achievable capacity [24]. For sensing, in turn, various

metrics are available, including the signal-to-interference-plus-noise ratio at the radar receiver (RX) [25], detection and false alarm probabilities [26], mutual information of the RX signal [27], different characteristics of the time-domain autocorrelation function, e.g., main-lobe width, peak side-lobe level (PSL) and the integrated side-lobe level [28], the PSL of the spatial waveform [29], [30], and the Cramer–Rao lower bounds (CRLBs) of the estimates [31].

Designing a JCAS waveform by minimizing the CRLB of range estimate is discussed in [32]. In contrast, in this article we jointly minimize both CRLBs of range and velocity estimates to design and optimize the joint waveform. Additionally, we consider standard-compliance aspects of practical mobile communication systems where the base station (BS) is utilized simultaneously for radar purposes while transmitting the downlink data modulated signal. Hence, the BS simultaneously acts as a joint radar transceiver (TRX) and communication TX with shared waveform. This is enabled by the assumed time-division duplexing (TDD) principle of the network [1] together with the full-duplex capability of the BS [33], allowing to measure and process the reflections from targets being illuminated by the TX waveform.

The main application framework in our work is 5G New Radio (NR) networks and their long-term evolution for enhanced JCAS support. Hence, stemming from the 5G NR standard [1], orthogonal frequency-division multiplexing (OFDM) is assumed as the baseline TX waveform, likely to be important also in 6G systems. In general, much research has already been done using the same OFDM waveform for sensing purposes, see, e.g., [34], [35]. Compared to other possible JCAS waveforms, e.g., linear frequency-modulated chirp [8] and cyclic prefixed single carrier [36], OFDM is of particular importance in mobile radio networks due to its natural support for multiple-input multiple-output (MIMO) processing and the resilience to frequency-selective fading through computationally efficient channel equalization methods. It is also helpful in sensing since it decouples the range and velocity estimation [8], while providing computationally efficient processing prospects. However, it has also selected drawbacks, e.g., high side-lobes in the range/velocity profiles, sensitivity to carrier-frequency offset, and high peak-to-average power ratio (PAPR) – something that we address along this work as part of the optimization framework.

In this work, we assume that the OFDM TX frame is not fully loaded, meaning that there are empty subcarriers that form the physical basis for the waveform optimization. Specifically, the empty subcarriers are filled using optimized frequency-domain samples to allow for improved sensing performance. Therefore, assuming that the total transmit power is constrained, some power of the communication subcarriers is effectively reallocated to these *radar subcarriers*, that basically controls the two subsystems' performance trade-off (fairness). Further, the amount of power reallocated can be decided by the BS according to the link budget. Specifically, the frequency-domain samples at the radar subcarriers are chosen by solving an optimization problem, such that they improve the accuracy of the delay and velocity estimation. We note that the radar subcarriers are transparent to the communication RX, that can simply discard them in the frequency domain data detection, and hence the approach does not influence the communication RX design.

It is also shortly noted that the assumed availability of empty subcarriers within the 5G NR physical downlink shared channel (PDSCH) depends on instantaneous network load and scheduling decisions. Interestingly, however, most of the mobile applications correspond to bursty data, and thus one can argue that the PDSCH resources are commonly not fully utilized. Additionally, other physical signal structures such as the downlink synchronization signal block (SSB) burst is standardized such that there are good amount of empty subcarriers [1] within the applicable OFDM symbols.

The scope and technical contributions of this article can be finally summarized as follows:

- Adapting CRLB expressions for range and velocity estimates found in existing literature, the solution to the joint optimization of the two CRLBs is derived analytically for an OFDM JCAS system to find the optimal radar subcarrier allocation.
- A computationally efficient algorithm is presented to find the solution to the joint optimization which provides the optimal trade-off between the delay and Doppler CRLBs.
- It is shown that the radar subcarriers' phases do not affect the joint optimization, hence allowing for further optimization of the TX waveform for PAPR minimization.
- The derived solutions to the optimization problems are numerically evaluated and validated through simulations in the timely 5G NR network context.
- We analyze the trade-off between the two subsystems and show that there is an optimum power allocation which allows both to function with sufficient performance.
- Finally, 5G NR waveforms with and without optimized radar subcarriers are used for RF measurements at 28 GHz band to sense and map an outdoor environment, showcasing the improvement of the range side-lobes in the radar image.

The rest of the paper is organized as follows. Section II describes the considered JCAS system model, together with the signal expressions for both subsystems. Section III outlines the general optimization problem, and the solution is derived analytically. A computationally feasible algorithm is also discussed for calculating the solution efficiently. Section IV then applies the proposed solutions in 5G NR system context, while providing a large collection of numerical results and their analysis. Section V concludes the main ideas of our research work. Finally, selected CRLB derivations and proofs are provided in Appendices A and B.

II. System Model

The considered JCAS system is shown in Fig. 1. The radar TRX is also a communication TX, which can feature multiple antenna arrays for TX and RX purposes, especially in case 5G and beyond networks operating at the mm-wave bands. The same OFDM waveform is utilized for both communication and sensing. The TX signal $x(t)$ is reflected from the targets

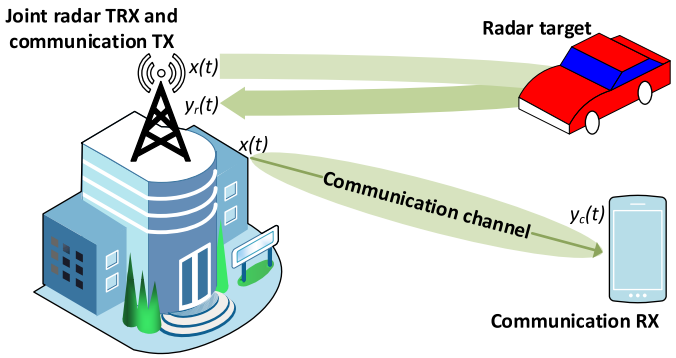

Fig. 1. The considered JCAS system model with the radar TRX and the communication TX, adopting the joint waveform.

in the environment and received back at the BS as $y_{\mathrm{r}}(t)$, and is used for detecting the targets. For this, the TX operates in a full-duplex manner [33]. The received signal at the communication RX is denoted by $y_{\mathrm{c}}(t)$.

The number of OFDM symbols for the whole waveform is denoted by M, with N denoting the number of active subcarriers per each symbol. The number of communication and radar subcarriers in the whole waveform are given by N_{c} and N_{r}, respectively, with $N_{\mathrm{c}}+N_{\mathrm{r}}=NM$. Additionally, the active communication subcarriers are divided into two classes—data and control—with their total number of subcarriers being N_{data} and N_{ctrl}, respectively, with $N_{\mathrm{data}}+N_{\mathrm{ctrl}}=N_{\mathrm{c}}$. The time–frequency indices of the control subcarriers are fixed, while those of data and radar subcarriers are uniformly distributed.

We note that both types of subcarriers are used for radar processing at the radar RX. So, even without any dedicated radar subcarriers in the waveform, targets can still be detected with only the communication subcarriers. This will, however, reduce the potential to improve the sensing performance with JCAS waveform optimization, as shown in Section IV. Additionally, the symbols on communication subcarriers are assumed to be fixed, whereas those on radar subcarriers can be modified.

The TX downlink signal is then given by

$$x(t)=\sum_{m\in\mathcal{M}}\frac{p(t-t_m)}{N}\Bigg(\sum_{n\in\mathcal{R}_m}X_{\mathrm{r},n,m}e^{j2\pi f_n(t-t_m)}+\sum_{n\in\mathcal{C}_m}X_{\mathrm{c},n,m}e^{j2\pi f_n(t-t_m)}\Bigg),\quad(1)$$

where the two separate inner summations correspond to the radar and communication subcarriers, respectively, while the outer summation is over the OFDM symbols. The n and m indices correspond to the subcarrier and OFDM symbol index, respectively, with $n\in[0,\ldots,N-1]$ and $m\in[0,\ldots,M-1]$.

The variables $p(t)$, $X_{\mathrm{r},n,m}$, $X_{\mathrm{c},n,m}$, f_n and t_m denote the pulse-shaping function, the TX symbol on a radar and communication subcarrier, frequencies of the subcarriers and the starting time instants of the OFDM symbols, respectively. Moreover, $\mathcal{R}_m$ and $\mathcal{C}_m$ are the radar and communication subcarrier indices for the m^{th} symbol, with $\mathcal{R}_m\cup\mathcal{C}_m=\mathcal{N}$, and $\mathcal{N}=\{n|n\in[0,\ldots,N-1]\}$. The set of OFDM symbols is given by $\mathcal{M}$, with $\mathcal{M}=\{m|m\in[0,\ldots,M-1]\}$. The total bandwidth of the signal is $f_{N-1}-f_0$ and the total signal duration is $t_{M-1}+\Delta t_{M-1}-t_0$, where Δt_{M-1} is the duration of last OFDM symbol. The frequencies and time instants are given by $f_n\in\{f_0,\ldots,f_{N-1}\}$ and $t_m\in\{t_0,\ldots,t_{M-1}\}$.

The instantaneous power for the radar and communication subcarriers over the whole waveform are

$$P_{\mathrm{r}}=\sum_{m\in\mathcal{M}}\sum_{n\in\mathcal{R}_m}P_{n,m},\quad P_{\mathrm{c}}=\sum_{m\in\mathcal{M}}\sum_{n\in\mathcal{C}_m}P_{n,m},\quad(2)$$

where $P_{n,m}=|X_{n,m}|^2$ represents the power of either subcarrier. Additionally, $P_{\mathrm{t}}=P_{\mathrm{r}}+P_{\mathrm{c}}$ denotes the total TX power.

A. Radar Subsystem

The received signal at the radar RX is given by

$$y_{\mathrm{r}}(t)=\sum_{k=1}^{K_{\mathrm{r}}}A_{\mathrm{r},k}x(t-\tau_{\mathrm{r},k})e^{j2\pi f_{\mathrm{r,D},k}t}+v_{\mathrm{r}}(t),\quad(3)$$

where K_{r}, $A_{\mathrm{r},k}$, $\tau_{\mathrm{r},k}$ and $f_{\mathrm{r,D},k}$ are the number of point targets in the environment, two-way attenuation constant between the radar TRX and a particular target (from the radar equation), delay to the target, and Doppler shift of the target, respectively. The additive white Gaussian noise (AWGN) at the radar RX $v_{\mathrm{r}}(t)$ is normally distributed with zero mean and σ_{r}^2 variance. The reflections from the k^{th} target will be received at the radar RX with a signal-to-noise ratio (SNR) of

$$\mathrm{SNR}_{\mathrm{r},k}=\frac{P_{\mathrm{t}}|A_{\mathrm{r},k}|^2}{\sigma_{\mathrm{r}}^2}.\quad(4)$$

Substituting (1) to (3) and performing the discrete Fourier transform (DFT) yields the relation between the TX and RX frequency-domain symbols $X_{n,m}$ and $Y_{\mathrm{r},n,m}$, respectively, as

$$Y_{\mathrm{r},n,m}=\sum_{k=1}^{K_{\mathrm{r}}}A_{\mathrm{r},k}X_{n,m}e^{-j2\pi f_n\tau_{\mathrm{r},k}}e^{j2\pi f_{\mathrm{r,D},k}t_m}+V_{\mathrm{r},n,m},\quad(5)$$

where the frequency-domain noise sample is denoted by $V_{\mathrm{r},n,m}$. This can be simplified for a single target as

$$Y_{\mathrm{r},n,m}=\underbrace{X_{n,m}e^{-j2\pi f_n\tau}e^{j2\pi t_m f_{\mathrm{D}}}}_{S_{n,m}}+V_{\mathrm{r},n,m},\quad(6)$$

showing that the delay and Doppler shift cause RX symbol's phase to differ from that of the TX symbol. Furthermore, the attenuation constant is normalized to unity while noise variance is scaled accordingly, but we do not introduce new symbols for $Y_{\mathrm{r},n,m}$ and $V_{\mathrm{r},n,m}$ in order to keep notation simple.

B. Delay and Doppler-Shift Estimation

Re-writing (6) in matrix form yields

$$\mathbf{Y}=\mathbf{DXB}+\mathbf{V},\quad(7)$$

where $\mathbf{Y}$ is the RX symbol matrix with $(\mathbf{Y})_{n,m}=Y_{\mathrm{r},n,m}$, $\mathbf{X}$ is the TX symbol matrix with $(\mathbf{X})_{n,m}=X_{n,m}$ and $\mathbf{V}$ is the noise matrix with $(\mathbf{V})_{n,m}=V_{\mathrm{r},n,m}$, all of the same size $N\times M$. The diagonal matrix $\mathbf{D}$ is of size $N\times N$ with $(\mathbf{D})_{n,n}=D_{n,n}=e^{-j2\pi f_n\tau}$. Similar diagonal matrix $\mathbf{B}$ is such that $(\mathbf{B})_{m,m}=B_{m,m}=e^{j2\pi t_m f_{\mathrm{D}}}$, of size $M\times M$.

The delay and Doppler shift of the target are then estimated using maximum likelihood estimation (MLE), given by

$$\boldsymbol{\theta} = [\tau, f_{\mathrm{D}}]^T, \tag{8}$$

where $\boldsymbol{\theta}$ is the set of parameters. For this, vectorizing (7) yields

$$\mathbf{y} = \mathbf{s} + \mathbf{v}, \tag{9}$$

where $\mathbf{y} = \mathrm{vec}(\mathbf{Y})$, $\mathbf{s} = \mathrm{vec}(\mathbf{DXB})$ and $\mathbf{v} = \mathrm{vec}(\mathbf{v})$ are all of the size $NM \times 1$, and $\mathrm{vec}(\cdot)$ is the vector operation. Vector $\mathbf{y}$ is assumed to be normally distributed with mean $\boldsymbol{\mu}$ and covariance $\boldsymbol{\Sigma}$, and

$$\boldsymbol{\mu} = \mathbb{E}\{\mathbf{y} - \mathbf{s}\} = \mathbf{0}, \tag{10}$$

$$\boldsymbol{\Sigma} = \mathbb{E}\{(\mathbf{y} - \mathbf{s})(\mathbf{y} - \mathbf{s})^H\} = \sigma_{\mathrm{r}}^2 \mathbf{I}, \tag{11}$$

where $\mathbf{0}$, $\mathbb{E}\{\cdot\}$ and $\mathbf{I}$ denote the zero vector, the expectation operation and the identity matrix, respectively.

The likelihood function of $\mathbf{y}$ can then be written as

$$\begin{aligned}\mathcal{P}_{\mathbf{y}}(\mathbf{y};\boldsymbol{\theta}) &= \frac{1}{|\boldsymbol{\Sigma}|\pi^{NM}} \exp\left(-(\mathbf{y}-\mathbf{s})^H \boldsymbol{\Sigma}^{-1}(\mathbf{y}-\mathbf{s})\right) \\ &= \frac{1}{\sigma_{\mathrm{r}}^2 \pi^{NM}} \exp\left(-\frac{(\mathbf{y}-\mathbf{s})^H(\mathbf{y}-\mathbf{s})}{\sigma_{\mathrm{r}}^2}\right). \end{aligned} \tag{12}$$

Taking the logarithm of (12) yields the log-likelihood function

$$\log \mathcal{P}_{\mathbf{y}}(\mathbf{y};\boldsymbol{\theta}) = -\log\left(\sigma_{\mathrm{r}}^2 \pi^{NM}\right) - \frac{(\mathbf{y}-\mathbf{s})^H(\mathbf{y}-\mathbf{s})}{\sigma_{\mathrm{r}}^2}. \tag{13}$$

Removing terms that do not depend on the parameters results in the simplified log-likelihood function as

$$\log \mathcal{P}'_{\mathbf{y}}(\mathbf{y};\boldsymbol{\theta}) = \Re\left(\mathbf{y}^H \mathbf{s}\right). \tag{14}$$

The estimated delay and Doppler shift, given by $\hat{\tau}$ and $\hat{f}_{\mathrm{D}}$, respectively, are found by maximizing (14) as

$$\max_{\boldsymbol{\theta}} \log \mathcal{P}'_{\mathbf{y}}(\mathbf{y};\boldsymbol{\theta}). \tag{15}$$

Consequently, $\hat{\boldsymbol{\theta}} = [\hat{\tau}, \hat{f}_{\mathrm{D}}]^T$ is the vector containing those two estimated parameters.

When the frequencies and time instants are uniformly spaced as $f_n = n\Delta f$ and $t_m = \frac{m}{\Delta f}$, where Δf denotes the frequency spacing, a grid-based method can be used to estimate the parameters. In this case, the simplified log-likelihood function in (14) can be re-written as

$$\log \mathcal{P}'_{\mathbf{Y}}(\mathbf{Y};\boldsymbol{\theta}) = \Re \sum_{m\in\mathcal{M}} \sum_{n\in\mathcal{N}} \tilde{Y}_{\mathrm{r},n,m} X_{n,m} e^{-j2\pi n \Delta f \tau} e^{\frac{j2\pi m f_{\mathrm{D}}}{\Delta f}}, \tag{16}$$

where $\tilde{Y}_{\mathrm{r},n,m}$ denotes the conjugate of $Y_{\mathrm{r},n,m}$. Then, quantizing the delay and Doppler parameters as

$$\tau_{n'} = \frac{n'}{N\Delta f}, \quad n' \in \mathcal{N}, \tag{17}$$

$$f_{\mathrm{D}m'} = \frac{m'\Delta f}{M}, \quad m' \in \mathcal{M}, \tag{18}$$

and substituting to (16) yields

$$\log \mathcal{P}'_{\mathbf{Y}}(n',m') = \Re\left[\overbrace{\sum_{m\in\mathcal{M}} \underbrace{\left(\sum_{n\in\mathcal{N}} Y'_{\mathrm{r},n,m} e^{\frac{-j2\pi n n'}{N}}\right)}_{\text{element } n' \text{in } N\text{-length DFT}} e^{\frac{j2\pi m m'}{M}}}^{\text{element } m' \text{in } M\text{-length IDFT}}\right], \tag{19}$$

where $Y'_{\mathrm{r},n,m} = \tilde{Y}_{\mathrm{r},n,m} X_{n,m}$. It is then observed that the inner and outer sums correspond to the DFT and inverse DFT (IDFT), respectively. As such, $n'_{\max}$ and $m'_{\max}$ are found as those values that maximize (19) as

$$\max_{n',m'} \log \mathcal{P}'_{\mathbf{Y}}(n',m'). \tag{20}$$

These are substituted back in (17) and (18) to yield the quantized delay and Doppler variables as

$$\hat{\boldsymbol{\theta}} = \left[\frac{n'_{\max}}{N\Delta f}, \frac{m'_{\max}\Delta f}{M}\right]^T. \tag{21}$$

C. Communication Subsystem

The RX signal at the communication RX is given by

$$y_{\mathrm{c}}(t) = h_{\mathrm{c}}(t) * x(t) + v_{\mathrm{c}}(t), \tag{22}$$

where $*$, $h_{\mathrm{c}}(t)$ and $v_{\mathrm{c}}(t)$ denote the convolution, impulse response of the communication channel and the AWGN noise at the communication RX with variance σ_{c}^2, respectively, and

$$h_{\mathrm{c}}(t) = \sum_{k=1}^{K_{\mathrm{c}}} A_{\mathrm{c},k} \delta(t - \tau_{\mathrm{c},k}) e^{j2\pi f_{\mathrm{c,D},k} t}. \tag{23}$$

Here, K_{c} and $A_{\mathrm{c},k}$ are the number of scatterers in the environment and the corresponding attenuation constant for the path between each scatterer and communication RX, $\tau_{\mathrm{c},k}$ and $f_{\mathrm{c,D},k}$ are the delay and Doppler shift of each scatterer, and $\delta(t)$ is the Dirac-delta function, respectively. In frequency domain, this can be written per each communication subcarrier as

$$H_{\mathrm{c},n,m} = \sum_{k=1}^{K_{\mathrm{c}}} A_{\mathrm{c},k} e^{-j2\pi f_n \tau_{\mathrm{c},k}} e^{j2\pi f_{\mathrm{c,D},k} t_m}, \tag{24}$$

where $H_{\mathrm{c},n,m}$ is assumed to remain constant for the duration of each OFDM symbol.

The RX symbols at the communication RX can then be written as

$$Y_{\mathrm{c},n,m} = H_{\mathrm{c},n,m} X_{\mathrm{c},n,m} + V_{\mathrm{c},n,m}, \tag{25}$$

where $Y_{\mathrm{c},n,m}$ and $V_{\mathrm{c},n,m}$ are the RX communication symbol and the frequency-domain noise sample, respectively. The capacity of the communication subcarriers is then given as

$$\beta_{\mathrm{c}} = \Delta f \sum_{m\in\mathcal{M}} \sum_{n\in\mathcal{C}_m} \log_2\left(1 + \frac{|H_{\mathrm{c},n,m}|^2 \,\mathbb{E}\{|X_{\mathrm{c},n,m}|^2\}}{\sigma_{\mathrm{c}}^2}\right). \tag{26}$$

TABLE I
OPTIMIZATION PARAMETERS

Parameter	Definition
ϕ	Maximum allowable CRLB($\hat{f}_{\mathrm{D}}$)
$P_{\max}$	Maximum power for a radar subcarrier
N_{act}	Number of activated radar subcarriers
P_{Δ}	Residual power allocated to one activated radar subcarrier
$\mathcal{R}_{m,\mathrm{act}}$	Set of subcarrier indices of the activated radar subcarriers in the m^{th} OFDM symbol
$\mathrm{SNR}_{\mathrm{r}}$	SNR at the radar RX
MS_f	Mean square bandwidth
MS_t	Mean square time
α	Communication loading ($\alpha = \frac{N_{\mathrm{data}}}{MN} \cdot 100\%$)
ΔPSD	Power spectral density difference between a radar and a communication subcarrier

III. Optimization of Radar Subcarriers

This section discusses the methodology by which the radar subcarriers are filled with optimized frequency-domain samples to improve the performance of the JCAS system. The optimization is performed in two stages: first for the radar subcarriers' amplitudes (or powers) and then for their phases.

A. Power Optimization for CRLB Minimization

For the sensing subsystem, the error variances of the estimated parameters in (21) need to be minimized in the ideal case, but for this, the explicit expressions of them cannot be found. Instead, the lower bounds for these error variances can be calculated easily, and are given by their CRLBs as

$$\mathrm{var}\{\hat{\tau}\} \geq \mathrm{CRLB}(\hat{\tau}), \quad \mathrm{var}\{\hat{f}_{\mathrm{D}}\} \geq \mathrm{CRLB}(\hat{f}_{\mathrm{D}}), \tag{27}$$

where $\mathrm{var}\{\cdot\}$ is the variance, $\mathrm{CRLB}(\hat{\tau})$ and $\mathrm{CRLB}(\hat{f}_{\mathrm{D}})$ denote the CRLB of the delay and Doppler estimate, respectively.

The CRLBs can be minimized, presuming that they also minimize the corresponding practical error variances. Later in the numerical results, we illustrate that such improvements are possible. For this, the radar subcarriers within the OFDM waveform are optimized such that they jointly minimize the delay and Doppler CRLBs. For the signal model in (6), these are derived in Appendix A, and given by (46)–(47b), indicating that they only depend on the amplitudes of the subcarriers and not their phases. Table I defines some important parameters necessary for the rest of the paper, in the order they appear in the text.

Optimization problem 1 (Joint Optimization): *The joint minimization of the delay and Doppler CRLBs aims at finding*

$$\min_{P_{n,m},\mathcal{R}_m} \mathrm{CRLB}(\hat{\tau}) \tag{28a}$$

$$\textit{subject to } \mathrm{CRLB}(\hat{f}_{\mathrm{D}}) \leq \phi, \tag{28b}$$

$$P_{\mathrm{r}} \leq P_{\mathrm{t}} - P_{\mathrm{c}}, \tag{28c}$$

$$0 \leq P_{n,m} \leq P_{\max}, \quad n \in \mathcal{R}_m, \ \forall m. \tag{28d}$$

Thus, $\mathrm{CRLB}(\hat{\tau})$ is minimized when $\mathrm{CRLB}(\hat{f}_{\mathrm{D}})$ is constrained to be below ϕ, where the power allocated to a radar subcarrier is limited by $P_{\max}$. The total radar power is based on the difference between the TX power and communication power. Here, we consider that P_{t} of the BS is known, as well as P_{c}. As such, P_{r} can be found readily, and the optimization intends to find the optimal powers $P_{n,m}$ for the individual radar subcarriers. Although the optimization minimizes the CRLBs of sensing, the performance of the communication subsystem can be kept at a satisfactory level by tuning P_{c}, which essentially controls the fairness between the two.

To solve this joint optimization problem, due to the very large search space of the subcarrier indices, optimal radar subcarrier indices receiving some power according to (28d) cannot be easily found. As such, a two-step process is applied for solving the optimization problem. Firstly, it is assumed that the optimal radar subcarrier indices are known. In that case, the solution is given by the following theorem.

Theorem 1: *In solving Optimization problem 1, there is an optimal set of radar subcarrier indices of cardinality N_{act}, out of which $N_{\mathrm{act}} - 1$ radar subcarriers are allocated a power of $P_{\max}$, while an additional radar subcarrier with indices $\{K, L\}$ is allocated remainder power P_{Δ}. The delay estimate's CRLB at this point is given by*

$$\mathrm{CRLB}(\hat{\tau}) = \phi \frac{\mathrm{NUM_c} + P_{\max} \sum_{m\in\mathcal{M}} \sum_{n\in\mathcal{R}_{m,\mathrm{act}}} \bar{t}_m^2 + \bar{t}_L^2 P_{\Delta}}{\mathrm{DEN_c} + P_{\max} \sum_{m\in\mathcal{M}} \sum_{n\in\mathcal{R}_{m,\mathrm{act}}} \bar{f}_n^2 + \bar{f}_K^2 P_{\Delta}}. \tag{29}$$

Here

$$\bar{f}_n = f_n - \frac{1}{N}\sum_{n\in\mathcal{N}} f_n, \ \bar{t}_m = t_m - \frac{1}{M}\sum_{m\in\mathcal{M}} t_m, \tag{30}$$

$$\mathrm{NUM_c} = \sum_{m\in\mathcal{M}} \sum_{n\in\mathcal{C}_m} \bar{t}_m^2 P_{n,m}, \ \mathrm{DEN_c} = \sum_{m\in\mathcal{M}} \sum_{n\in\mathcal{C}_m} \bar{f}_n^2 P_{n,m}, \tag{31}$$

$$N_{\mathrm{act}} = \left\lceil \frac{P_{\mathrm{t}} - P_{\mathrm{c}}}{P_{\max}} \right\rceil, \tag{32}$$

$$P_{\Delta} = P_{\mathrm{t}} - P_{\mathrm{c}} - P_{\max}\left(N_{\mathrm{act}} - 1\right), \tag{33}$$

where $\lceil . \rceil$ is the ceiling operation, and N_{act} is the number of activated radar subcarriers needed to satisfy the total radar power constraint. Due to the ceiling operation in (32), one radar subcarrier will receive a lesser power than $P_{\max}$, which is given by P_{Δ}. The set of activated radar subcarriers for the m^{th} OFDM symbol is denoted by $\mathcal{R}_{m,\mathrm{act}}$.

Proof: See Appendix B. □

The next step in solving the joint optimization is to find the set of N_{act} activated radar subcarriers out of all the possible radar subcarriers. Since the possible combinations for the activated radar subcarriers are given by $\binom{N_r}{N_{\mathrm{act}}}$, the search space is still huge. To reduce this, optimal radar subcarrier indices for the separate optimizations of $\mathrm{CRLB}(\hat{\tau})$ and $\mathrm{CRLB}(\hat{f}_{\mathrm{D}})$ are utilized to derive the optimal indices for the joint optimization. These optimization approaches are described next.

Optimization problem 2 (Separate Minimization):

(a) $\min_{P_{n,m},\mathcal{R}_m} \mathrm{CRLB}(\hat{\tau})$ *subject to* $P_{\mathrm{r}} \leq P_{\mathrm{t}} - P_{\mathrm{c}}$, *and* $0 \leq P_{n,m} \leq P_{\max}, \ n \in \mathcal{R}_m, \forall m$,

(b) $\min_{P_{n,m},\mathcal{R}_m} \mathrm{CRLB}(\hat{f}_{\mathrm{D}})$ *subject to* $P_{\mathrm{r}} \leq P_{\mathrm{t}} - P_{\mathrm{c}}$, *and* $0 \leq P_{n,m} \leq P_{\max}, \ n \in \mathcal{R}_m, \forall m$.

The optimal radar subcarrier indices for the two separate CRLB optimizations are then given by the following theorem.

Theorem 2: *The activated radar subcarrier indices for separate minimization of* $\text{CRLB}(\hat{\tau})$ *and* $\text{CRLB}(\hat{f}_\text{D})$ *are respectively given by the edge-most radar subcarriers in frequency domain and edge-most OFDM symbols in time domain.*

Proof: When only one parameter in (8) needs to be estimated, Fisher information matrix will also have one element, given by (43) for $i = j = 1$. For the two estimates, these are given separately by (45a) and (45c), and the CRLBs are then

$$\text{CRLB}(\hat{\tau})_\text{sep} = \frac{1}{8\pi^2(\text{SNR}_\text{r})} \cdot \underbrace{\frac{1}{\left(\text{DEN}_\text{c} + P_\text{max} \sum_{m\in\mathcal{M}} \sum_{n\in\mathcal{R}_{m,\text{act}}} \bar{f}_n^2 + \bar{f}_K^2 P_\Delta\right)}}_{\text{MS}_f} \tag{34}$$

and

$$\text{CRLB}(\hat{f}_\text{D})_\text{sep} = \frac{1}{8\pi^2(\text{SNR}_\text{r})} \cdot \underbrace{\frac{1}{\left(\text{NUM}_\text{c} + P_\text{max} \sum_{m\in\mathcal{M}} \sum_{n\in\mathcal{R}_{m,\text{act}}} \bar{t}_m^2 + \bar{t}_L^2 P_\Delta\right)}}_{\text{MS}_t}. \tag{35}$$

Here, $\text{CRLB}(\hat{\tau})_\text{sep}$ and $\text{CRLB}(\hat{f}_\text{D})_\text{sep}$ are the minimum CRLBs when optimal radar subcarrier indices are used, and to find these, separate optimizations are performed as in Optimization problem 2.

From (34), to minimize $\text{CRLB}(\hat{\tau})$, MS_f should be maximized. Hence, the edge-most $N_\text{act} - 1$ radar subcarriers (maximum $\bar{f}_n^2$) are allocated P_max, while the N_act^th edge-most radar subcarrier is allocated P_Δ.

From (35), to minimize $\text{CRLB}(\hat{f}_\text{D})$, MS_t should be maximized. Hence, all radar subcarriers of the edge-most OFDM symbols (maximum $\bar{t}_m^2$) are allocated P_max, while also for some radar subcarriers in the least edge-most OFDM symbol, depending on N_act. In that OFDM symbol, a single radar subcarrier is allocated P_Δ. □

Due to the joint estimation, both the CRLBs are degraded w.r.t. the separate estimations, as observed from (47a) and (47b). To find the optimal radar subcarrier indices for the joint optimization, those for the separate delay optimization are then used as a starting point to reduce the complexity of the search space. A computationally efficient algorithm for this task is provided by the following theorem.

Theorem 3: *The optimal radar subcarrier indices for the joint optimization can be efficiently calculated by the Algorithm 1.*

Proof: The two CRLBs are inversely related as in (48). Hence

$$\min \text{CRLB}(\hat{\tau}) \implies \max \text{MS}_f, \tag{36}$$

$$\min \text{CRLB}(\hat{f}_\text{D}) \implies \max \text{MS}_t. \tag{37}$$

The minimum $\text{CRLB}(\hat{\tau})$ is given by (34), and it represents the case when MS_f is the maximum. This is the starting point of the algorithm. Let the frequency-domain symbols on N_move $(\leq N_\text{act})$ activated radar subcarriers with indices $\{n'_a, m'_a\}$, $a \in [1, N_\text{move}]$ be moved to unactivated radar subcarriers with indices $\{n_a, m_a\}$. The maximum MS_f is then

$$\text{MS}_f = \text{DEN}_\text{c} + P_\text{max} \sum_{m\in\mathcal{M}} \sum_{n\in\mathcal{R}_{m,\text{act}}} \bar{f}_n^2 + \bar{f}_K^2 P_\Delta + P_\text{max} \sum_{a=2}^{N_\text{move}} \left(\bar{f}_{n_a}^2 - \bar{f}_{n'_a}^2\right) + P_\Delta(\bar{f}_{n_1}^2 - \bar{f}_{n'_1}^2). \tag{38}$$

Similarly from (35), the MS_t at this point is

$$\text{MS}_t = \text{NUM}_\text{c} + P_\text{max} \sum_{m\in\mathcal{M}} \sum_{n\in\mathcal{R}_{m,\text{act}}} \bar{t}_m^2 + \bar{t}_L^2 P_\Delta + P_\text{max} \sum_{a=2}^{N_\text{move}} \left(\bar{t}_{m_a}^2 - \bar{t}_{m'_a}^2\right) + P_\Delta(\bar{t}_{m_1}^2 - \bar{t}_{m'_1}^2). \tag{39}$$

For least degradation of MS_f, the indices n'_a are chosen such that they have the least frequencies $\bar{f}_{n'_a}$ out of all the activated radar subcarriers, while the indices n_a are the next highest frequencies $\bar{f}_{n_a}$, out of all the unactivated radar subcarriers, ensuring that $\left(\bar{f}_{n_a}^2 - \bar{f}_{n'_a}^2\right)$ is degraded the least.

Once the subcarrier indices for the activated radar subcarriers are found, the next step is to choose the OFDM symbols for them. Following a similar logic, from (39) it can be deduced that the indices m'_a should have the least time instants $\bar{t}_{m'_a}$ out of all the activated radar subcarriers, while m_a should have the next highest time instants $\bar{t}_{m_a}$, for the remaining unactivated radar subcarriers. This ascertains that $\left(\bar{t}_{m_a}^2 - \bar{t}_{m'_a}^2\right)$ is maximized as much as possible. This is done until all N_act radar subcarriers are moved. In the end, this would generate the waveform with the highest MS_t, viz. the waveform when only Doppler estimation is performed.

For the same number of activated radar subcarriers moved N_move, better CRLBs cannot be found than the ones provided by the algorithm since for any other combination of radar subcarrier and OFDM symbol indices, either $\left(\bar{f}_{n_a}^2 - \bar{f}_{n'_a}^2\right)$ or $\left(\bar{t}_{m_a}^2 - \bar{t}_{m'_a}^2\right)$ will be less than the one provided by Algorithm 1, which ensures that the two CRLBs reside on the Pareto curve. This completes the proof. □

Algorithm 1 Joint Optimization Algorithm

Set $i = 0$
Initialize $\mathcal{R}_{\text{act},i}$ to be the edge-most radar subcarriers
Set $\mathcal{R}_{\text{act,new},i} = \varnothing$
while $i \leq N_\text{act}$ **do**
  Compute $\text{CRLB}(\hat{\tau})_i$ and $\text{CRLB}(\hat{f}_\text{D})_i$
  Select the activated radar subcarrier having the minimum $\bar{f}_n$, with indices $\{n_\text{min}, m_\text{min}\}$
  Select the unactivated radar subcarrier having the maximum $\bar{f}_n$ on the maximum $\bar{t}_m$ time instant, with indices $\{n_\text{max}, m_\text{max}\}$
  Set $X_{\text{r},n_\text{max},m_\text{max}} = X_{\text{r},n_\text{min},m_\text{min}}$
  Set $X_{\text{r},n_\text{min},m_\text{min}} = 0$
  $\mathcal{R}_{\text{act},i+1} = \mathcal{R}_{\text{act},i} \setminus \{n_\text{min}, m_\text{min}\}$
  $\mathcal{R}_{\text{act,new},i+1} = \mathcal{R}_{\text{act,new},i} \cup \{n_\text{max}, m_\text{max}\}$
  $i \leftarrow i + 1$

The i variable in the algorithm denotes the number of active radar subcarriers moved from MS_f to MS_t maximization. Thus, each $\text{CRLB}(\hat{\tau})_i$ and $\text{CRLB}(\hat{f}_\text{D})_i$ correspond to the trade-off between the CRLBs of the two estimates and $\text{CRLB}(\hat{\tau})_0$ and $\text{CRLB}(\hat{f}_\text{D})_{N_\text{act}}$ correspond to the CRLB values when the waveform is only optimized separately for either optimization. Once the indices of the activated radar subcarriers are found (contingent on the indices of the communication subcarriers), depending on i, their amplitudes are given readily as $\sqrt{P_\text{max}}$ (or P_Δ). As such, the computational complexity is low for the amplitude optimization of the activated radar subcarriers.

B. Phase Optimization for PAPR Minimization

Since the CRLBs depend only on the amplitudes, the phases can be optimized separately to minimize PAPR that is notoriously high for default OFDM waveforms [37]. Hence, the phases of activated radar subcarriers are optimized to reduce the PAPR in our work [30], [38]. To reduce the complexity, phase optimization is done for each OFDM symbol to reduce that particular symbol's PAPR, which allows to reduce the PAPR of the whole waveform.

The PAPR of the m^th OFDM symbol is

$$\text{PAPR}_{x_m[a]} = 10\log_{10}\frac{\max\{|x_m[a]|^2\}}{\mathbb{E}\{|x_m[a]|^2\}}, \tag{40}$$

where $x_m[a]$ is the sampled sequence of the m^th OFDM symbol's time-domain waveform, based on $x(t)$ in (1). Here, $a \in [0, N_\text{IDFT}-1]$ and N_IDFT is the IDFT size for one OFDM symbol, and $\max\{\cdot\}$ is the maximum operation. The phase optimization can then be denoted as below.

Optimization problem 3 (Phase optimization of activated radar subcarriers): *We aim to find* $\min_{\boldsymbol{\zeta}_m} \text{PAPR}_{x_m[a]}$, *where* $\boldsymbol{\zeta}_m$ *is the set of phases for the activated radar subcarriers in the* m^th *OFDM symbol, while* $\boldsymbol{\zeta}_{\text{opt},m}$ *denotes the corresponding optimum phases.*

To solve Optimization problem 3, selective mapping (SLM) is used in this article [39]. Thus, U sets of random phases are chosen for the activated radar subcarriers of each OFDM symbol. For the m^th OFDM symbol, these are given as $\mathbf{Z}_m = [\boldsymbol{\zeta}_{0,m}, \ldots, \boldsymbol{\zeta}_{U-1,m}]$, $u \in [0, U-1]$, with $\mathbb{C}\{\boldsymbol{\zeta}_{u,m}\} = \mathbb{C}\{\mathcal{R}_{m,\text{act}}\}$, where $\mathbb{C}\{\cdot\}$ is the cardinality.

This operation thus produces U possible waveforms for each OFDM symbol, and these can be given based on (1) as

$$x_m^u(t) = \frac{p(t-t_m)}{N}\Bigg(\sum_{n\in\mathcal{C}_m} X_{\text{c},n,m}e^{j2\pi f_n(t-t_m)} + P_\text{max}\sum_{n\in\mathcal{R}_{m,\text{act}}} e^{j2\pi\zeta_{u,n,m}}e^{j2\pi f_n(t-t_m)}\Bigg), \tag{41}$$

where $\zeta_{u,n,m} = (\boldsymbol{\zeta}_{u,m})_n$, and $x_m^u(t)$ is the u^th time-domain waveform of the m^th OFDM symbol. Since the U sets of phases are random, the PAPR of each waveform is different, and one set of phases will produce the minimum PAPR. These are found by solving Optimization problem 3. This is repeated for all the OFDM symbols to minimize the PAPR of the whole TX waveform. This PAPR minimization scheme is summarized in Algorithm 2.

Algorithm 2 Phase Optimization Algorithm

```
Set m = 0, u = 0
while m ≤ M − 1 do
    while u ≤ U − 1 do
        Set ζ_{u,m} as uniformly distributed random numbers
        between [0, 1]
        For n ∈ R_{m,act}, set X_{r,n,m} = P_max e^{j2πζ_{u,n,m}}
        Compute the PAPR of the OFDM symbol (40)
        u ← u + 1
    Set ζ_{opt,m} using Optimization problem 3
    For n ∈ R_{m,act}, set X_{r,n,m} = P_max e^{j2π(ζ_{opt,m})_n}
    m ← m + 1
```

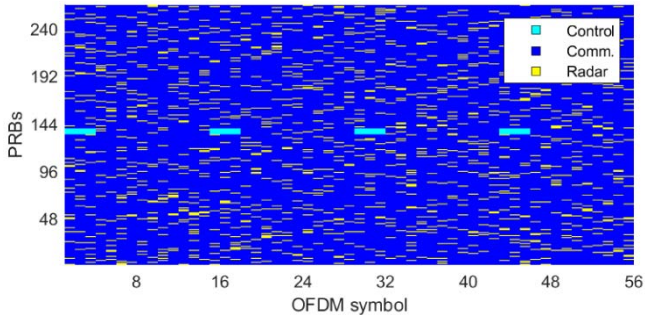

Fig. 2. Resource grid showing the distribution of different PRBs of the considered 5G NR waveform for $M = 56$ and $\alpha = 90\%$.

For Algorithm 2, the search space is massive and an exhaustive search is infeasible to be performed. Hence, the solution obtained is suboptimal in comparison to the global optimum. Additionally, this cannot be performed in a real-time system, while finding computationally more efficient solutions to facilitate real-time processing is an important future research topic. However, in this work, we demonstrate the general prospects of also optimizing the phases of the activated radar subcarriers for PAPR minimization. Further, any other method which optimizes the phases of the subcarriers can be readily applied for PAPR minimization, instead of the SLM approach used herein, e.g., a modified version of the method adopted in [40].

IV. Numerical Results

A 5G NR waveform is used for the simulations with parameters: $M = 560$, total bandwidth of 400 MHz, $\Delta f = 120$ kHz and centered around $f_c = 28$ GHz. For this bandwidth, the number of physical resource blocks (PRBs) is 264 with $N = 3168$ subcarriers [41]. The total duration of the frame is 0.5 ms and the TX power is used at 30 dBm.

The resource grid in frequency domain is depicted in Fig. 2, for a communication loading α of 90%, with $\alpha = \frac{N_\text{data}}{MN}\cdot 100\%$. It shows the distribution of different PRBs. The control PRBs recur for every slot (14 OFDM symbols) and span over three OFDM symbols, with six PRBs. Within each communication PRB, there exist two pilot subcarriers. The communication subcarriers constitute quadrature phase-shift keying symbols, while the pilots are binary phase-shift keying symbols. Each OFDM symbol has a fixed number of radar subcarriers.

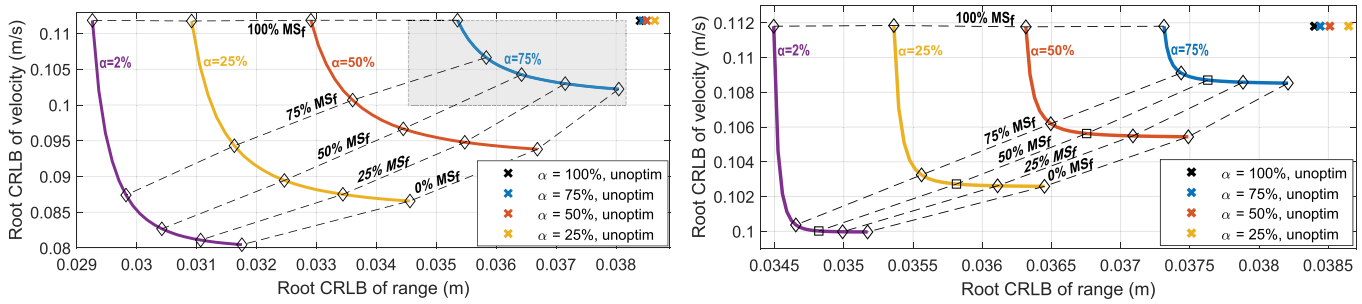

(a) ΔPSD $= 3$ dB (b) ΔPSD $= 1$ dB

Fig. 3. Trade-off between range and velocity root CRLBs for different α and MS_f %, for (a) ΔPSD $= 3$ dB and (b) 1 dB, when activated radar subcarriers are moved. The grey rectangle in (a) depicts the area corresponding to (b). When $\alpha = 2\%$ and unoptimized, that corresponds to the point $(0.0438, 0.1119)$.

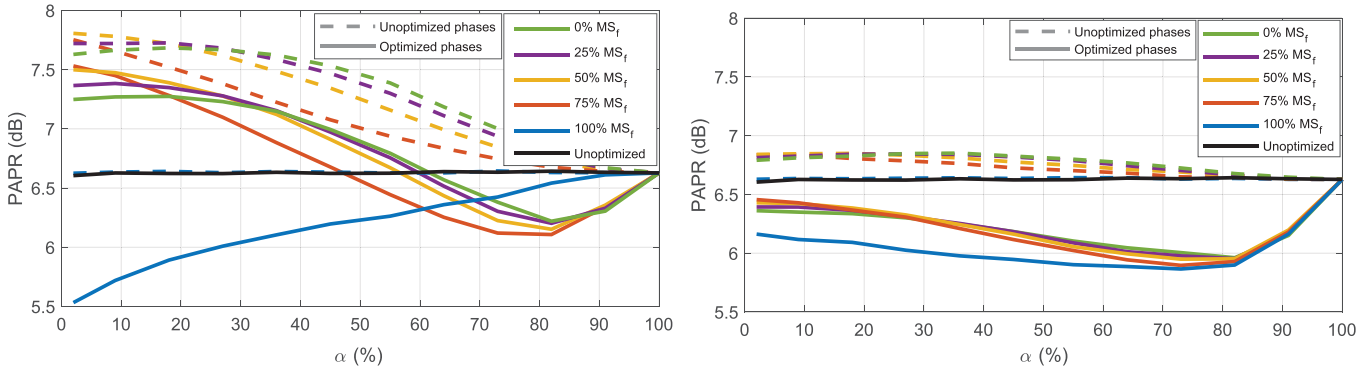

(a) ΔPSD $= 3$ dB (b) ΔPSD $= 1$ dB

Fig. 4. The effect of optimizing phases of the activated radar subcarriers on the PAPR of waveforms, for different α, and (a) ΔPSD $= 3$ dB and (b) 1 dB.

A. Simulation Results

Figure 3 shows the results for the joint CRLB optimization. The delay and Doppler values are converted to range and velocity, with the use of $\hat{d} = \frac{c\hat{\tau}}{2}$ and $\hat{v} = \frac{c\hat{f}_\text{D}}{2f_c}$, where $\hat{d}$, $\hat{v}$ and c are the range estimate, velocity estimate, and speed of light, respectively. The power spectral density (PSD) difference (ΔPSD) between a radar and communication subcarrier is maintained at two values, 3 dB and 1 dB, and these cases are denoted by Figs. 3(a) and 3(b), respectively.

For the optimized waveform, when α decreases, both CRLBs also decrease. This is because with decreased α, number of radar subcarriers increases, and it gives more degrees of freedom for the optimization. Comparing between the two figures, reduced CRLBs are observed for the higher ΔPSD. Increasing this value increases the power allocated to a radar subcarrier (P_max), and from (32), this will reduce the number of active radar subcarriers. This allows maximizing either the MS_f or MS_t as required. Both figures also show the CRLBs of the unoptimized waveform, where the radar subcarriers are empty, and the communication subcarriers use all the available power. Therefore, reallocating some power from the communication subcarriers to the radar subcarriers allows to minimize the CRLBs in comparison with the case when the total power is allocated to the communication subcarriers.

Since the starting point of Algorithm 1 is the optimized waveform with maximum MS_f, radar power is allocated to those radar subcarriers at the edges of the spectrum. To improve MS_t, some active radar subcarriers at the edges of the spectrum can be moved to the edge OFDM symbols, which in turn decreases MS_f. Thus, when MS_f % decreases, the CRLB of range increases, while that of velocity decreases, which depicts the inherent trade-off between the two CRLBs. Here, MS_f % denotes $100\% - \frac{i}{N_\text{act}} \cdot 100\%$ in Algorithm 1.

The effect of optimizing the radar subcarriers' phases on the PAPR is shown in Figs. 4(a) and 4(b), for ΔPSD $=$ 3 dB and 1 dB, and $U = 50$. Here and in the subsequent figures, the default 5G waveform without any radar subcarriers is denoted as *unoptimized* (black curve). Instead of using pure random phases as in Algorithm 2, the chosen random phases are further iterated using the `fminunc` function of the optimization toolbox of MATLAB. This was done to lower the required U than that is needed from pure randomization, but which also depicts sufficient PAPR improvement. Then, the phases that give the minimum PAPR are chosen as the optimum phases.

The *unoptimized phases* cases denote the waveforms where the locations and amplitudes of activated radar subcarriers are optimized to minimize the CRLBs, but their phases are not, being simply uniformly distributed within $[0, 2\pi]$. In these waveforms, when MS_f % decreases, the number of activated radar subcarriers in the edge OFDM symbols increases, while in the center OFDM symbols, they will be decreased. Consequently, these waveforms will have more power allocated

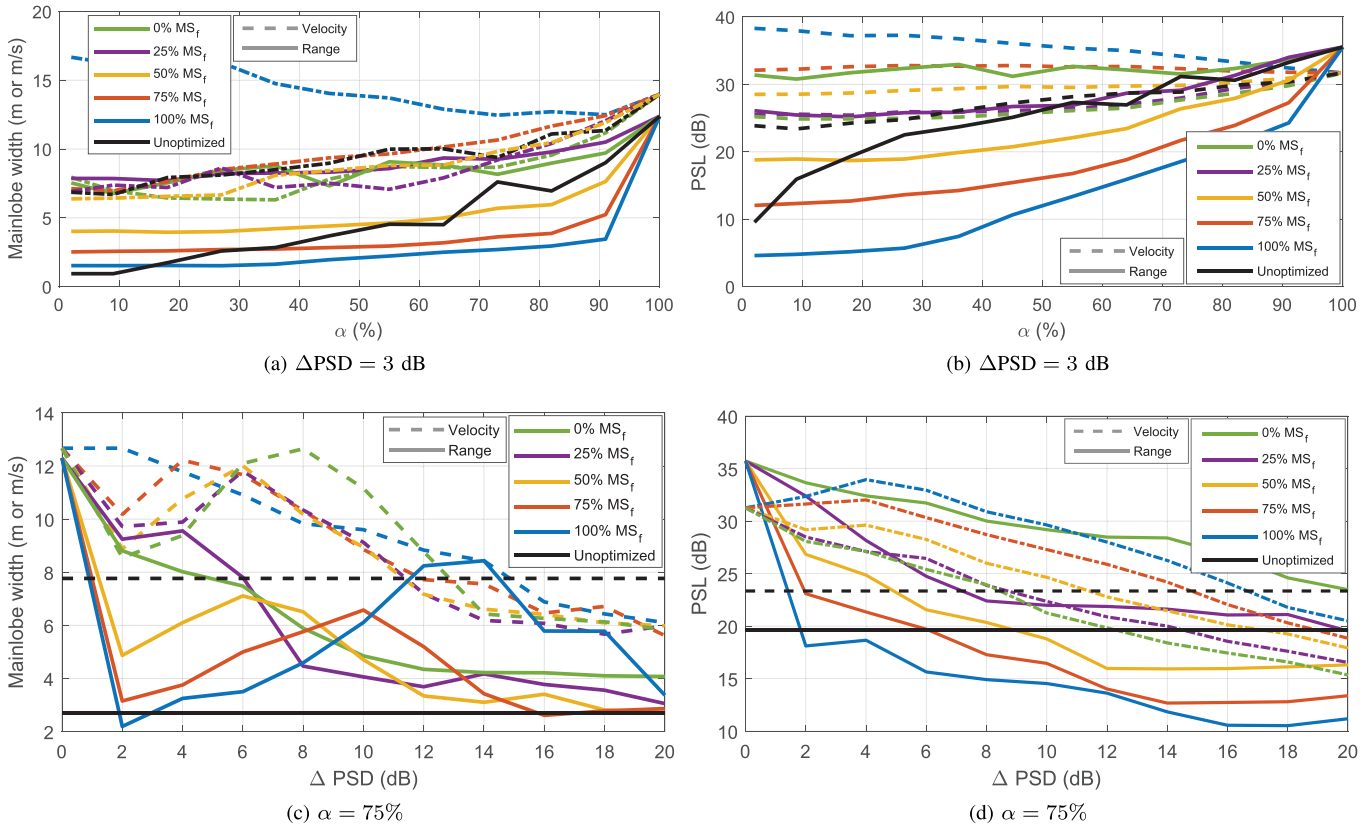

(a) ΔPSD $= 3$ dB (b) ΔPSD $= 3$ dB

(c) $\alpha = 75\%$ (d) $\alpha = 75\%$

Fig. 5. Comparison between the main-lobe widths and PSLs, for fixed ΔPSD $= 3$ dB shown in (a) and (b), and for fixed $\alpha = 75\%$, shown in (c) and (d).

to the edges of the time-domain signal than for the center. Although the average power of the time-domain signal remains the same, this results in the peak power of the edge OFDM symbols to increase. Thus, these waveforms will then have higher peak power than that of the default 5G waveform, whereas the average power is the same for both. This is the reason for the PAPR to increase in the phase unoptimized cases compared to the default 5G waveform. The same analogy can be applied as the reason for the PAPR to increase when MS_f % decreases in both phase unoptimized and optimized cases.

Comparing between the Figs. 4(a) and 4(b), it can be observed that when ΔPSD increases, the PAPR increases. This is because when $P_{\max}$ increases, the number of activated radar subcarriers in (32) decreases, and hence the peak power of the time-domain signal increases even more. Further, the PAPR decreases with the increase of α, due to the reduction of the activated radar subcarriers in the edge OFDM symbols. However, phase optimization is observed to reduce the PAPR, indicating the feasibility of numerically optimizing the phases of the activated radar subcarriers.

To evaluate the improved performance in a practical scenario, simulations are performed by placing a point target with varying velocity at different ranges. Then, the optimized joint waveform is used as the TX waveform, and the reflected RX signal is used for target detection. Next, MLE is performed to estimate the range and relative velocity of the target. The main-lobe width and PSL of the target in range and velocity profiles are also then calculated. This is performed for many iterations to obtain the average performance.

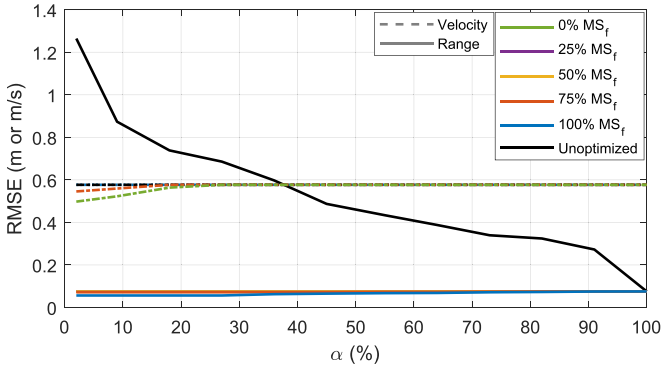

Fig. 6. The RMSEs of range and velocity for $\text{SNR}_\text{r} = -10$ dB and ΔPSD $=$ 3 dB, for unoptimized and optimized waveforms.

Figure 5(a) depicts the main-lobe widths of the peak corresponding to the detected target, in both range and velocity, for ΔPSD $= 3$ dB, which are calculated as the null-to-null distance of the main-lobe peak. The range profile's main-lobe width decreases when either α decreases or MS_f % increases, i.e., when more radar subcarriers are available for MS_f maximization, the target can be made narrower in the range domain. Additionally, the main-lobe width of the optimized waveform can be lowered compared to that of the unoptimized waveform, depending on α and MS_f %. Similarly for the velocity, having more radar subcarriers for MS_t maximization (lower MS_f %), improves its main-lobe width, while marginally better main-lobe width can be obtained than that of

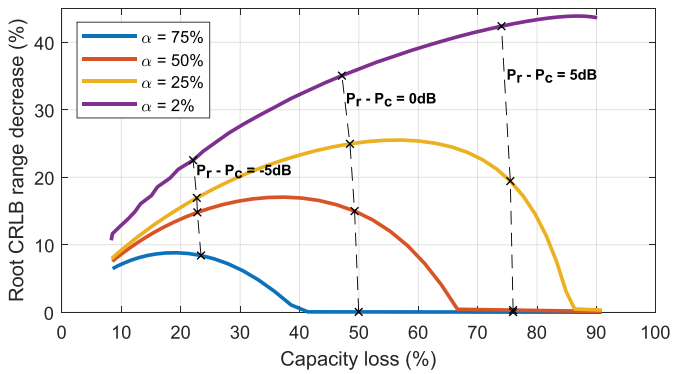

(a) Communication capacity and root CRLB range, for 100% MS_f

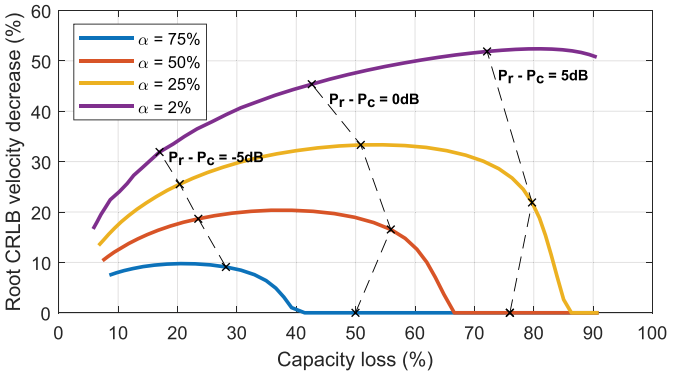

(b) Communication capacity and root CRLB velocity, for 0% MS_f

Fig. 7. Trade-off between communication capacity and two CRLBs for different α and $\Delta\text{PSD} = 3$ dB, when $P_\text{r} - P_\text{c}$ is varied between -10 dB and 10 dB.

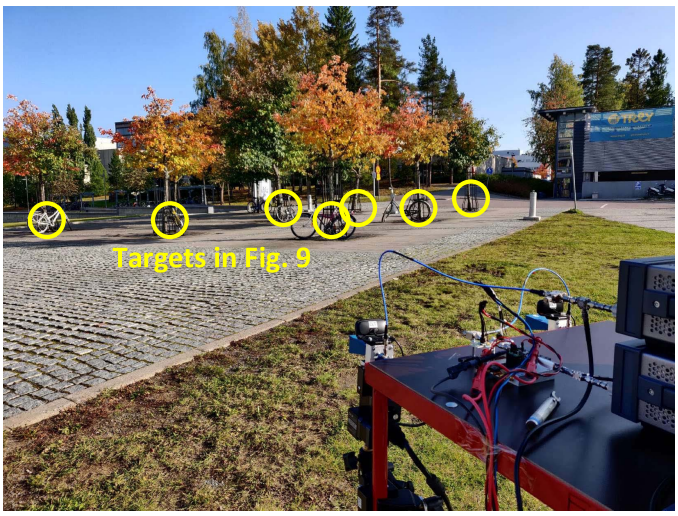

(a) Mapped outdoor environment

(b) Equipment used in the measurement setup

Fig. 8. The outdoor sensing and mapping scenario indicating the targets in the environment, and the hardware measurement setup, which emulates the joint radar TRX at 27.7 GHz.

the corresponding unoptimized waveform. So, the target can be made narrower in range or velocity domains by allocating radar subcarriers for either MS_f or MS_t maximization.

Figure 5(b) illustrates the PSLs for both range and velocity, for $\Delta\text{PSD} = 3$ dB. The PSL is calculated as the difference between the main-lobe peak and the next peak within 40 samples, and a higher PSL is thus suitable for target detection. The range profile's PSL decreases when either α decreases (increase of radar power) or MS_f % increases (more radar power for MS_f maximization). When either of these happens, most of the radar power is pushed to the edges of the spectrum, increasing the ambiguity in range domain. For the velocity profile, its PSL decreases when MS_f % decreases. Hence, this maximizes MS_t by pushing more power towards the edge OFDM symbols, thereby increasing the ambiguity in velocity profile. To summarize, allocating radar power to either the edges of frequency or time increases the ambiguity in the corresponding range and velocity profiles. However, by varying MS_f % for a given α, either profile's PSL can be improved by properly allocating the active radar subcarriers, outperforming the corresponding unoptimized waveform.

Next, the variation of main-lobe width of both profiles is analyzed for different ΔPSD values, when α is fixed at 75%, with the results depicted in Fig. 5(c). The main-lobe widths in the figure are calculated as null-to-null distance while averaging over different point targets and TX frequency-domain symbol realizations. This results in somewhat wild variations, however, a general observation is that for both profiles, when ΔPSD passes some threshold value for a given MS_f %, the main-lobe width decreases, and for certain combinations, they can be made lower than that of the unoptimized waveform.

Figure 5(d) depicts the variation of PSLs of both profiles with ΔPSD, for a fixed $\alpha = 75\%$. An increase of ΔPSD is observed to generally decrease the PSLs of both profiles. Doing that increases P_max and from (32), the number of active radar subcarriers is decreased. Since the radar power is fixed due to fixed α, all that power is distributed among a lesser number of active radar subcarriers. Hence, more power is pushed to the edges of either the frequency spectrum or the time-domain waveform, increasing MS_f or MS_t, respectively. Following a similar analogy as for Fig. 5(b), the corresponding

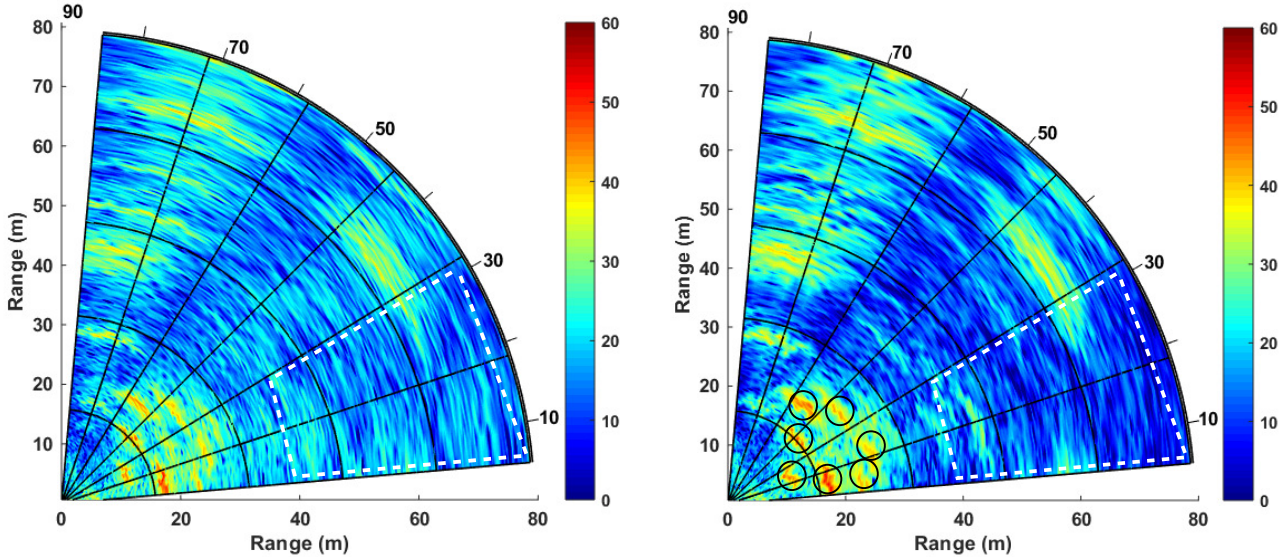

(a) Unoptimized waveform (b) Optimized waveform

Fig. 9. The outdoor environment mapped with the unoptimized and the optimized standard compliant 5G NR waveforms at 27.7 GHz, for $\alpha = 25\%$ and $\Delta\text{PSD} = 3$ dB. Waveform bandwidth is 400 MHz.

PSLs of the profiles decrease accordingly. By suitably choosing ΔPSD for a given MS_f %, however, allows to increase the PSL behavior beyond that of the unoptimized waveform.

The root mean square errors (RMSEs) of both range and velocity estimates are next calculated, and Fig. 6 shows these results for $\text{SNR}_\text{r} = -10$ dB. For both estimates, optimized waveforms have lower RMSEs than those of the corresponding unoptimized waveforms. Moreover, the improvement is clearly visible for the range estimate. Therefore, optimizing the waveform based on the theoretical CRLBs also enables to achieve performance improvement in a practical scenario.

To evaluate communication subsystem's performance, a multipath channel is simulated with free-space path loss of 121.4 dB, and RX noise power of -87.1 dBm. The communication capacity of the communication subcarriers is then calculated based on (26). Since some power is taken away from the communication subcarriers to fill the radar subcarriers, there will be a trade-off between each subsystem's performance with the power allocation $P_\text{r} - P_\text{c}$. Figures 7(a) and 7(b) depict this in terms of the communication capacity and the two CRLBs, when $P_\text{r} - P_\text{c}$ is varied. Further, the percentages of CRLB decrease/capacity loss denote the improvement/degradation w.r.t. the unoptimized cases.

Both figures show that the CRLB improvement reaches a maximum, decreasing there onward. When $P_\text{r} - P_\text{c}$ increases, more power is allocated for the radar subcarriers. Depending on P_max, there is a maximum number of active radar subcarriers in the waveform, and once all of them are allocated P_max, there will be a residual power of $P_\text{t} - P_\text{c} - P_\text{max}\,(N_\text{act} - 1) - P_\Delta$ that is reallocated to the communication subcarriers. As such, this will reduce the CRLB improvement.

The optimum power allocation $P_\text{r} - P_\text{c}$ for CRLB improvement would thus be at the maximum point of each curve. Increasing the power allocation beyond that would be detrimental for both subsystems. Moreover, this power allocation is less for higher α values. In that case, less number of radar subcarriers exist, and less radar power is required. Therefore, these two figures depict the trade-off between the two subsystems, and depending on α, power allocation can also be varied for optimum performance.

B. Measurement Results at 28 GHz Band

To observe and illustrate the performance in a practical measurement-based scenario, the unoptimized and optimized waveforms are next used to sense and map a real-world outdoor environment. This section discusses the related measurement setup and the scenario, while also illustrating the results.

1) Measurement Campaign and the Scenario: Figure 8(a) depicts the measurement scenario, with static targets highlighted (bicycles near some metallic structures). A vector signal transceiver (VST) of model PXIe-5840 is used for TX and RX processing at an intermediate frequency of 3.2 GHz. Two mixers of model N5183B-MXG, operating at 24.5 GHz are used at both ends of the VST to up/down-convert the signals to/from the mm-wave frequency of 27.7 GHz. Standard-compliant 5G NR waveform with 400 MHz channel bandwidth is utilized, without and with the optimized radar subcarriers. As the TX and RX antennas, two horn antennas of model PE9851A-20 are used to emulate the joint radar TRX, with a 3-dB beamwidth of 17° and a gain of 20 dBi. Having these directional beams emulate phased arrays, and allow to compensate for the high attenuation evident in the mm-wave frequencies. These antennas are then mechanically steered between 5° and 85° directions with a step size of 2°. A trolley is used to mount the two antennas and carry all

the equipment. Two power amplifiers are also used at the TX chain. This setup is shown in Fig. 8(b).

2) Sensing Results: Since only static targets are sensed, the waveform with 100% of activated radar subcarriers for MS_f is used as the optimized TX signal, with ΔPSD of 3 dB. Further, $M = 20$ OFDM symbols are used, but the other parameters are the same as used in the simulations. For each angle, range estimation is performed for the 20 OFDM symbols, and they are coherently combined to obtain a single range profile. These are then used to generate the map of the outdoor environment.

Figure 9(a) shows these mapping results for the unoptimized waveform, with $\alpha = 25\%$, while Fig. 9(b) shows the corresponding results when the waveform is optimized. The targets in Fig. 8(a) are also circled in Fig. 9(b) for better understanding and visualization of the environment. Comparing between the two figures (e.g., highlighted area for 40–80m and 0–30°), it is clearly observed that the optimized waveform enables to considerably minimize range side-lobes in the radar image, indicating that allocating power for the radar subcarriers has allowed clearly identifying the detected targets. Additionally, the overall clutter level is clearly reduced. Therefore, though the optimization is based on minimizing the theoretical CRLB of the range estimate, it shows promising results in a practical scenario as well. More comprehensive measurement results and assessment are available in our related work in [20].

V. Conclusion

This article addressed the OFDM waveform optimization for 5G–6G JCAS systems. Empty subcarriers within the waveform are filled with optimized frequency-domain samples to improve the radar subsystem's performance, by reallocating a portion of the communication subcarriers' power. The results indicate that the CRLBs and RMSEs of range and velocity, as well as the transmit waveform PAPR can be efficiently controlled and minimized through the described optimization approaches. Further, the optimization is shown to narrow the main-lobe widths of the range and velocity profiles, at the cost of decreasing their PSLs. However, by properly selecting the optimization parameters, improved performance is observed when compared with the corresponding unoptimized waveform. Additionally, the trade-off between the subsystems indicates that the power allocation can be chosen intelligently for optimal performance of both subsystems. Finally, over-the-air RF measurements were performed at 28 GHz, with both optimized and unoptimized 5G NR waveforms, for an outdoor environment sensing mapping scenario to demonstrate the range side-lobe improvement due to the optimization.

Appendix A
CRLB Expressions for the OFDM Signal Model

Here, we derive the expressions for the delay and Doppler CRLBs, using the Fisher information matrix, for the OFDM signal model.

When the parameter estimation is considered to be unbiased, $\int(\hat{\boldsymbol{\theta}} - \boldsymbol{\theta})\mathcal{P}_{\mathbf{y}}(\mathbf{y};\boldsymbol{\theta})dy = \mathbf{0}$, where $\mathcal{P}_{\mathbf{y}}(\mathbf{y};\boldsymbol{\theta})$ is centered around the zero vector. Differentiating w.r.t. $\boldsymbol{\theta}$, it can be restated as $\mathbb{E}\{(\hat{\boldsymbol{\theta}} - \boldsymbol{\theta})\frac{\partial \log \mathcal{P}_{\mathbf{y}}(\mathbf{y};\boldsymbol{\theta})}{\partial \boldsymbol{\theta}}^T\} = \mathbf{I}$. Pre/post-multiplying this by $\mathbf{w}^T$ and $\mathcal{I}^{-1}(\boldsymbol{\theta})\mathbf{w}$ respectively, where $\mathbf{w}$ is an arbitrary vector and $\mathcal{I}(\boldsymbol{\theta})$ is the Fisher information matrix, and using the Cauchy–Schwarz inequality yields $(\mathbf{w}^T\mathcal{I}^{-1}(\boldsymbol{\theta})\mathbf{w})^2 \leq \mathbf{w}^T\text{cov}(\hat{\boldsymbol{\theta}})\mathbf{w} \cdot \mathbf{w}^T\mathcal{I}^{-1}(\boldsymbol{\theta})\mathcal{I}(\boldsymbol{\theta})\mathcal{I}^{-1}(\boldsymbol{\theta})\mathbf{w}$. Simplifying it results in the matrix $\text{cov}(\hat{\boldsymbol{\theta}}) - \mathcal{I}^{-1}(\boldsymbol{\theta})$ being positive semi-definite, where $\text{cov}(\hat{\boldsymbol{\theta}}) = \mathbb{E}\{(\hat{\boldsymbol{\theta}} - \boldsymbol{\theta})(\hat{\boldsymbol{\theta}} - \boldsymbol{\theta})^T\}$ denotes the covariance matrix of the zero-mean estimates.

Additionally, each element of $\mathcal{I}(\boldsymbol{\theta})$ is given by $\mathcal{I}(\boldsymbol{\theta})_{i,j} = \mathbb{E}\left(\frac{\partial \log \mathcal{P}_{\mathbf{y}}(\mathbf{y};\boldsymbol{\theta})}{\partial \boldsymbol{\theta}_i}\frac{\partial \log \mathcal{P}_{\mathbf{y}}(\mathbf{y};\boldsymbol{\theta})}{\partial \boldsymbol{\theta}_j}\right)$, where i and j are the row and column numbers of the matrix. Then, CRLBs of delay and Doppler estimates are given by the diagonal elements of $\mathcal{I}^{-1}(\boldsymbol{\theta})$ as [42]

$$\text{CRLB}(\hat{\tau}) = \frac{\mathcal{I}(\boldsymbol{\theta})_{2,2}}{\det\{\mathcal{I}(\boldsymbol{\theta})\}}, \quad \text{CRLB}(\hat{f}_{\text{D}}) = \frac{\mathcal{I}(\boldsymbol{\theta})_{1,1}}{\det\{\mathcal{I}(\boldsymbol{\theta})\}}, \tag{42}$$

where $\det\{\cdot\}$ represents the determinant. Using the definition of the second derivative and some simplifying analysis steps, each element of $\mathcal{I}(\boldsymbol{\theta})$ can be restated as

$$\mathcal{I}(\boldsymbol{\theta})_{i,j} = -\mathbb{E}\left\{\frac{\partial^2 \log \mathcal{P}_{\mathbf{y}}(\mathbf{y};\boldsymbol{\theta})}{\partial \boldsymbol{\theta}_i \partial \boldsymbol{\theta}_j}\right\}. \tag{43}$$

Substituting $\mathcal{P}_{\mathbf{y}}(\mathbf{y};\boldsymbol{\theta})$ from (13) and using (10), (43) then becomes $\mathcal{I}(\boldsymbol{\theta})_{i,j} = \left(\frac{2}{\sigma_{\text{r}}^2}\right)\Re\left(\frac{\partial \mathbf{s}^H}{\partial \boldsymbol{\theta}_i}\frac{\partial \mathbf{s}}{\partial \boldsymbol{\theta}_j}\right)$. After performing the two partial differentiations, this can next be written in the form of

$$\mathcal{I}(\boldsymbol{\theta})_{i,j} = \frac{2}{\sigma_{\text{r}}^2}\Re\left(\mathbf{s}^H\mathbf{D}_{\boldsymbol{\theta}_i}^H\mathbf{D}_{\boldsymbol{\theta}_j}\mathbf{s}\right). \tag{44}$$

Here, $\mathbf{D}_{\theta_1} = (-j2\pi)\text{diag}(\mathbf{d}_\tau)$, in which $\mathbf{d}_\tau$ is of size $NM \times 1$, where the first N elements are $[\bar{f}_0, \bar{f}_{N-1}]$, and being repeated for M times. Similarly, $\mathbf{D}_{\theta_2} = (j2\pi)\text{diag}(\mathbf{d}_{f_{\text{D}}})$, in which $\mathbf{d}_{f_{\text{D}}}$ is of size $NM \times 1$ where sets of M elements are the same, with the starting and ending indices being $\bar{t}_0$ and $\bar{t}_{M-1}$, respectively. Mean-shifted frequency and time variables are used since $\mathcal{P}_{\mathbf{y}}(\mathbf{y};\boldsymbol{\theta})$ is centered around zero. Elements of the Fisher information matrix are then

$$\begin{aligned}
\mathcal{I}(\boldsymbol{\theta})_{1,1} &= \frac{8\pi^2}{\sigma_{\text{r}}^2}\sum_{m\in\mathcal{M}}\sum_{n\in\mathcal{N}}\bar{f}_n^2|S_{n,m}|^2 \\
&= 8\pi^2(\text{SNR}_{\text{r}})\sum_{m\in\mathcal{M}}\sum_{n\in\mathcal{N}}\bar{f}_n^2 P_{n,m} \\
&= 8\pi^2(\text{SNR}_{\text{r}})(\text{MS}_f), \qquad (45a) \\
\mathcal{I}(\boldsymbol{\theta})_{1,2} &= \mathcal{I}(\boldsymbol{\theta})_{2,1} = -8\pi^2(\text{SNR}_{\text{r}})\sum_{m\in\mathcal{M}}\sum_{n\in\mathcal{N}}\bar{t}_m\bar{f}_n P_{n,m} \\
&= -8\pi^2(\text{SNR}_{\text{r}})(\text{MS}_{f,t}), \qquad (45b) \\
\mathcal{I}(\boldsymbol{\theta})_{2,2} &= 8\pi^2(\text{SNR}_{\text{r}})\sum_{m\in\mathcal{M}}\sum_{n\in\mathcal{N}}\bar{t}_m^2 P_{n,m} \\
&= 8\pi^2(\text{SNR}_{\text{r}})(\text{MS}_t), \qquad (45c)
\end{aligned}$$

where $\frac{|S_{n,m}|^2}{P_{\text{t}}} = P_{n,m}$, and $\text{MS}_{f,t}$ is the mean square bandwidth–time. Using (42), the two CRLBs are given as

$$\begin{aligned}
\text{CRLB}(\hat{\tau}) &= \frac{1}{8\pi^2(\text{SNR}_{\text{r}})f(\mathbf{P})}, \\
\text{CRLB}(\hat{f}_{\text{D}}) &= \frac{1}{8\pi^2(\text{SNR}_{\text{r}})g(\mathbf{P})},
\end{aligned} \tag{46}$$

where

$$f(\mathbf{P}) = (\mathrm{MS}_f) - \frac{(\mathrm{MS}_{f,t})^2}{(\mathrm{MS}_t)} = \sum_{m\in\mathcal{M}}\sum_{n\in\mathcal{N}} \bar{f}_n^2 P_{n,m} - \frac{\left(\sum_{m\in\mathcal{M}}\sum_{n\in\mathcal{N}} \bar{t}_m \bar{f}_n P_{n,m}\right)^2}{\sum_{m\in\mathcal{M}}\sum_{n\in\mathcal{N}} \bar{t}_m^2 P_{n,m}}, \tag{47a}$$

$$g(\mathbf{P}) = (\mathrm{MS}_t) - \frac{(\mathrm{MS}_{f,t})^2}{(\mathrm{MS}_f)}, \tag{47b}$$

where the CRLBs are in a similar format as those in [43].

Appendix B
Proof of Theorem 1

Here, the solution to Optimization problem 1 is derived. Substituting for $\mathrm{MS}_{f,t}$ from (47a) to (47b) gives $\frac{g(\mathbf{P})}{f(\mathbf{P})} = \frac{\mathrm{MS}_t}{\mathrm{MS}_f}$. Using this relation in (46) then results in

$$\frac{\mathrm{CRLB}(\hat{\tau})}{\mathrm{CRLB}(\hat{f}_\mathrm{D})} = \frac{\mathrm{MS}_t}{\mathrm{MS}_f}. \tag{48}$$

Since the right-hand side of this equation denotes an inverse relation, it can be deduced that the two CRLBs also have an inverse relationship. Hence, for the minimum value of $\mathrm{CRLB}(\hat{\tau})$ in Optimization problem 1, the value of $\mathrm{CRLB}(\hat{f}_\mathrm{D})$ should be maximized. This means that the inequality constraint in (28b) simplifies into an equality constraint.

Differentiating $\mathrm{CRLB}(\hat{\tau})$ in (46) w.r.t. the power of a general radar subcarrier with indices $\{k,l\}$ results in

$$\frac{\partial \mathrm{CRLB}(\hat{\tau})}{\partial P_{k,l}} = \left(\frac{-1}{8\pi^2(\mathrm{SNR}_\mathrm{r})}\right) \cdot \left(\frac{\bar{f}_k - \frac{\bar{t}_l \sum_{m\in\mathcal{M}}\sum_{n\in\mathcal{N}} \bar{t}_m \bar{f}_n P_{n,m}}{\sum_{m\in\mathcal{M}}\sum_{n\in\mathcal{N}} \bar{t}_m^2 P_{n,m}}}{f(\mathbf{P})}\right)^2 \leq 0. \tag{49}$$

We next address the condition for which $\frac{\partial \mathrm{CRLB}(\hat{\tau})}{\partial P_{k,l}} = 0$. Specifically, this happens when

$$\frac{\bar{f}_k}{\bar{t}_l} = \frac{\sum_{m\in\mathcal{M}}\sum_{n\in\mathcal{N}} \bar{t}_m \bar{f}_n P_{n,m}}{\sum_{m\in\mathcal{M}}\sum_{n\in\mathcal{N}} \bar{t}_m^2 P_{n,m}} = \frac{\mathrm{MS}_{f,t}}{\mathrm{MS}_t}, \tag{50}$$

where (45b) and (45c) are used to arrive at $\frac{\mathrm{MS}_{f,t}}{\mathrm{MS}_t}$. This ratio is fixed for a given waveform and does not necessarily become exactly equal to $\frac{\bar{f}_k}{\bar{t}_l}$. Even at the extremely unlikely case where it does, it happens only for one $\{k,l\}$ pair, and not for all radar subcarriers. Hence, this means that $\frac{\partial \mathrm{CRLB}(\hat{\tau})}{\partial P_{k,l}} < 0$, and therefore $\mathrm{CRLB}(\hat{\tau})$ always decreases when a radar subcarrier's power increases. Hence, the minimum is found when the power constraint in (28c) is satisfied with equality: $P_\mathrm{r} = P_\mathrm{t} - P_\mathrm{c}$. Thus, inequality constraints (28b) and (28c) simplify into equality constraints.

Based on (48), the relation between the two CRLBs can be written also using (45a) and (45c) as

$$\mathrm{CRLB}(\hat{\tau}) = \left(\mathrm{CRLB}(\hat{f}_\mathrm{D})\right) \frac{\sum_{m\in\mathcal{M}}\sum_{n\in\mathcal{N}} \bar{t}_m^2 P_{n,m}}{\sum_{m\in\mathcal{M}}\sum_{n\in\mathcal{N}} \bar{f}_n^2 P_{n,m}} = \left(\mathrm{CRLB}(\hat{f}_\mathrm{D})\right) \eta(\mathbf{P}). \tag{51}$$

The derivatives of $\mathrm{CRLB}(\hat{f}_\mathrm{D})$ and $\eta(\mathbf{P})$ will be necessary for solving the optimization problem. They are given below by using (46) and (51) respectively as

$$\frac{\partial \mathrm{CRLB}(\hat{f}_\mathrm{D})}{\partial P_{k,l}} = \left(\frac{-1}{8\pi^2(\mathrm{SNR}_\mathrm{r})}\right) \cdot \left(\frac{\bar{t}_l - \frac{\bar{f}_k \sum_{m\in\mathcal{M}}\sum_{n\in\mathcal{N}} \bar{t}_m \bar{f}_n P_{n,m}}{\sum_{m\in\mathcal{M}}\sum_{n\in\mathcal{N}} \bar{f}_n^2 P_{n,m}}}{g(\mathbf{P})}\right)^2 < 0, \tag{52}$$

$$\frac{\partial \eta(\mathbf{P})}{\partial P_{k,l}} = \frac{\bar{t}_l^2}{\sum_{m\in\mathcal{M}}\sum_{n\in\mathcal{N}} \bar{f}_n^2 P_{n,m}} - \frac{\bar{f}_k^2 \sum_{m\in\mathcal{M}}\sum_{n\in\mathcal{N}} \bar{t}_m^2 P_{n,m}}{\left(\sum_{m\in\mathcal{M}}\sum_{n\in\mathcal{N}} \bar{f}_n^2 P_{n,m}\right)^2}. \tag{53}$$

To solve the optimization problem in (28a)–(28d), the Lagrangian function is used [44], and can be denoted as

$$\begin{aligned} Q(\mathbf{P},\zeta,\boldsymbol{\beta},\boldsymbol{\gamma},\delta) &= \left(\mathrm{CRLB}(\hat{f}_\mathrm{D})\right)\eta(\mathbf{P}) \\ &\quad + \zeta\left(P_\mathrm{t} - P_\mathrm{c} - \sum_{l\in\mathcal{M}}\sum_{k\in\mathcal{R}_l} P_{k,l}\right) \\ &\quad + \sum_{l\in\mathcal{M}}\sum_{k\in\mathcal{R}_l} \beta_{k,l}(P_\mathrm{max} - P_{k,l}) - \sum_{l\in\mathcal{M}}\sum_{k\in\mathcal{R}_l} \gamma_{k,l} P_{k,l} \\ &\quad + \delta\left(\phi - \mathrm{CRLB}(\hat{f}_\mathrm{D})\right), \end{aligned} \tag{54}$$

where the objective function $\mathrm{CRLB}(\hat{\tau})$ is replaced by $\left(\mathrm{CRLB}(\hat{f}_\mathrm{D})\right)\eta(\mathbf{P})$ using (51). Here, $\zeta, \boldsymbol{\beta}, \boldsymbol{\gamma}$ and δ are the Karush–Kunn–Tucker (KKT) multiplier corresponding to the total radar power constraint, matrices of KKT multipliers corresponding to the upper and lower bounds of power for the individual radar subcarriers and the KKT multiplier corresponding to the CRLB of the Doppler estimate, respectively. To have an optimal solution, the KKT conditions should be satisfied, which are given as

$$\frac{\partial Q(\mathbf{P},\zeta,\boldsymbol{\beta},\boldsymbol{\gamma},\delta)}{\partial P_{k,l}} = \left(\mathrm{CRLB}(\hat{f}_\mathrm{D})\right)\frac{\partial \eta(\mathbf{P})}{\partial P_{k,l}} + (\eta(\mathbf{P}) - \delta) \times \frac{\partial \mathrm{CRLB}(\hat{f}_\mathrm{D})}{\partial P_{k,l}} - \zeta - \beta_{k,l} - \gamma_{k,l} = 0, \tag{55}$$

$$\beta_{k,l}(P_\mathrm{max} - P_{k,l}) = 0, \tag{56}$$

$$\gamma_{k,l} P_{k,l} = 0, \tag{57}$$

$$\beta_{k,l} \geq 0, \tag{58}$$

$$\gamma_{k,l} \geq 0, \tag{59}$$

$$\sum_{l\in\mathcal{M}}\sum_{k\in\mathcal{R}_l} P_{k,l} = P_\mathrm{t} - P_\mathrm{c}, \tag{60}$$

$$\mathrm{CRLB}(\hat{f}_\mathrm{D}) = \phi, \tag{61}$$

$$P_{k,l} \leq P_\mathrm{max}, \tag{62}$$

$$P_{k,l} \geq 0. \tag{63}$$

Defining two sets for the cases when the radar subcarriers are activated and not activated, respectively, as

$$\mathbf{Z}_\beta = \{\{k,l\}|\beta_{k,l} \neq 0\}, \tag{64}$$

$$\mathbf{Z}_\gamma = \{\{k,l\}|\gamma_{k,l} \neq 0\}, \tag{65}$$

where from (56), $\mathbf{Z}_\beta$ is the set of radar subcarriers for which $P_{k,l} = P_{\max}$ (activated), while from (57), $\mathbf{Z}_\gamma$ is the set of radar subcarriers for which $P_{k,l} = 0$ (unactivated). Further, $\mathbf{Z}_\beta \cap \mathbf{Z}_\gamma = \varnothing$.

$N_{act} \geq N_r$*:* In this case, all radar subcarriers are activated and receive $P_{\max}$. If $N_{\text{act}} P_{\max} > P_{\text{t}} - P_{\text{c}}$, the residual power is reallocated to the communication subcarriers. Some special cases can also arise, such as when $N_{\text{act}} - 1 = N_{\text{r}}$, the total radar power is exactly divided among all the radar subcarriers, while when $N_{\text{act}} = N_{\text{r}}$, all but one subcarrier receive $P_{\max}$ power, while the remaining power is given to the last. These are uninteresting cases, and much attention is given to the cases when the number of activated radar subcarriers is less when compared with the total radar subcarriers.

$N_{act} < N_r$*:* The expression in (55) needs to be satisfied for all the k and l values. It is clear that when $\mathbf{Z}_\beta = \varnothing$ and $\mathbf{Z}_\gamma = \varnothing$, it cannot be satisfied for all the radar subcarriers. Thus, at least one $\{k,l\}$ dependent β or γ parameter (either the radar subcarrier should receive $P_{\max}$ or zero power) should exist. Evaluating KKT conditions for all these possible cases of $\beta_{k,l}$ and $\gamma_{k,l}$,

$\mathbf{Z}_\beta = \varnothing, \mathbb{C}\{\mathbf{Z}_\gamma\} = N_r$*:* All radar subcarriers are empty and the radar power constraint is not satisfied.

$\mathbb{C}\{\mathbf{Z}_\beta\} = z, \mathbb{C}\{\mathbf{Z}_\gamma\} = N_r - z,\ z \in [1, N_{act} - 1]$*:* z radar subcarriers are active with $P_{k,l} = P_{\max}$ power. Since $\sum_{l\in\mathcal{M}} \sum_{k\in\mathcal{R}_l} P_{k,l} < P_{\text{t}} - P_{\text{c}}$, power constraint is not satisfied.

$\mathbb{C}\{\mathbf{Z}_\beta\} = N_{act}, \mathbb{C}\{\mathbf{Z}_\gamma\} = N_r - N_{act}$*:* The power requirement is met exactly (no fractional part due to the division in (32)), and much attention is given to the next, which represents a practical situation.

$\mathbb{C}\{\mathbf{Z}_\beta\} = N_{act} - 1, \mathbb{C}\{\mathbf{Z}_\gamma\} = N_r - N_{act}$*:* Here $N_{\text{act}} - 1$ radar subcarriers receive the maximum power, while an additional radar subcarrier receives a power of $P_{K,L} = P_\Delta$. This denotes the feasible solution to this optimization problem and the function value at this point is given by (29).

REFERENCES

[1] H. Holma, A. Toskala, and T. Nakamura, *5G Technology: 3GPP New Radio*. Hoboken, NJ, USA: Wiley, 2019.

[2] F. Liu, C. Masouros, A. P. Petropulu, H. Griffiths, and L. Hanzo, "Joint radar and communication design: Applications, state-of-the-art, and the road ahead," *IEEE Trans. Commun.*, vol. 68, no. 6, pp. 3834–3862, Jun. 2020.

[3] J. H. Reed *et al.*, "On the co-existence of TD-LTE and radar over 3.5 GHz band: An experimental study," *IEEE Wireless Commun. Lett.*, vol. 5, no. 4, pp. 368–371, Aug. 2016.

[4] M. Ghorbanzadeh, E. Visotsky, P. Moorut, W. Yang, and C. Clancy, "Radar inband and out-of-band interference into LTE macro and small cell uplinks in the 3.5 GHz band," in *Proc. IEEE Wireless Commun. Netw. Conf. (WCNC)*, Mar. 2015, pp. 1829–1834.

[5] B. D. Cordill, S. A. Seguin, and L. Cohen, "Electromagnetic interference to radar receivers due to in-band OFDM communications systems," in *Proc. IEEE Int. Symp. Electromagn. Compat.*, Aug. 2013, pp. 72–75.

[6] F. Hessar and S. Roy, "Spectrum sharing between a surveillance radar and secondary Wi-Fi networks," *IEEE Trans. Aerosp. Electron. Syst.*, vol. 52, no. 3, pp. 1434–1448, Jun. 2016.

[7] Q. Zhao and A. Swami, "A survey of dynamic spectrum access: Signal processing and networking perspectives," in *Proc. IEEE Int. Conf. Acoust., Speech Signal Process. (ICASSP)*, vol. 4, Apr. 2007, pp. 1349–1352.

[8] B. Paul, A. R. Chiriyath, and D. W. Bliss, "Survey of RF communications and sensing convergence research," *IEEE Access*, vol. 5, pp. 252–270, 2017.

[9] C. De Lima *et al.*, "Convergent communication, sensing and localization in 6G systems: An overview of technologies, opportunities and challenges," *IEEE Access*, vol. 9, pp. 26902–26925, Jan. 2021.

[10] D. Ma, N. Shlezinger, T. Huang, Y. Liu, and Y. C. Eldar, "Joint radar-communication strategies for autonomous vehicles: Combining two key automotive technologies," *IEEE Signal Process. Mag.*, vol. 37, no. 4, pp. 85–97, Jul. 2020.

[11] F. Liu and C. Masouros, "A tutorial on joint radar and communication transmission for vehicular networks—Part I: Background and fundamentals," *IEEE Commun. Lett.*, vol. 25, no. 2, pp. 322–326, Feb. 2021.

[12] F. Liu and C. Masouros, "A tutorial on joint radar and communication transmission for vehicular networks—Part II: State of the art and challenges ahead," *IEEE Commun. Lett.*, vol. 25, no. 2, pp. 327–331, Feb. 2021.

[13] F. Liu and C. Masouros, "A tutorial on joint radar and communication transmission for vehicular networks—Part III: Predictive beamforming without state models," *IEEE Commun. Lett.*, vol. 25, no. 2, pp. 332–336, Feb. 2021.

[14] J. Andrew Zhang *et al.*, "Enabling joint communication and radar sensing in mobile networks–a survey," 2020, *arXiv:2006.07559*. [Online]. Available: http://arxiv.org/abs/2006.07559

[15] A. R. Chiriyath, B. Paul, and D. W. Bliss, "Radar-communications convergence: Coexistence, cooperation, and co-design," *IEEE Trans. Cognit. Commun. Netw.*, vol. 3, no. 1, pp. 1–12, Mar. 2017.

[16] C. B. Barneto *et al.*, "High-accuracy radio sensing in 5G new radio networks: Prospects and self-interference challenge," in *Proc. 53rd Asilomar Conf. Signals, Syst., Comput.*, Nov. 2019, pp. 1159–1163.

[17] M. L. Rahman, J. A. Zhang, X. Huang, Y. J. Guo, and R. W. Heath, "Framework for a perceptive mobile network using joint communication and radar sensing," *IEEE Trans. Aerosp. Electron. Syst.*, vol. 56, no. 3, pp. 1926–1941, Jun. 2020.

[18] P. Kumari, J. Choi, N. Gonzalez-Prelcic, and R. W. Heath, "IEEE 802.11Ad-based radar: An approach to joint vehicular communication-radar system," *IEEE Trans. Veh. Technol.*, vol. 67, no. 4, pp. 3012–3027, Apr. 2018.

[19] H. Wymeersch, G. Seco-Granados, G. Destino, D. Dardari, and F. Tufvesson, "5G mmWave positioning for vehicular networks," *IEEE Wireless Commun.*, vol. 24, no. 6, pp. 80–86, Dec. 2017.

[20] S. D. Liyanaarachchi, C. B. Barneto, T. Riihonen, and M. Valkama, "Experimenting joint vehicular communications and sensing with optimized 5G NR waveform," in *Proc. IEEE 93rd Veh. Technol. Conf. (VTC-Spring)*, Apr. 2021, pp. 1–5.

[21] C. B. Barneto, T. Riihonen, M. Turunen, M. Koivisto, J. Talvitie, and M. Valkama, "Radio-based sensing and indoor mapping with millimeter-wave 5G NR signals," in *Proc. Int. Conf. Localization GNSS (ICL-GNSS)*, Jun. 2020, pp. 1–5.

[22] A. R. Chiriyath, B. Paul, G. M. Jacyna, and D. W. Bliss, "Inner bounds on performance of radar and communications co-existence," *IEEE Trans. Signal Process.*, vol. 64, no. 2, pp. 464–474, Jan. 2016.

[23] P. Kumari, S. A. Vorobyov, and R. W. Heath, "Adaptive virtual waveform design for millimeter-wave joint communication–radar," *IEEE Trans. Signal Process.*, vol. 68, pp. 715–730, 2020.

[24] K. V. Mishra, M. R. Bhavani Shankar, V. Koivunen, B. Ottersten, and S. A. Vorobyov, "Toward millimeter-wave joint radar communications: A signal processing perspective," *IEEE Signal Process. Mag.*, vol. 36, no. 5, pp. 100–114, Sep. 2019.

[25] A. Aubry, A. De Maio, Y. Huang, M. Piezzo, and A. Farina, "A new radar waveform design algorithm with improved feasibility for spectral coexistence," *IEEE Trans. Aerosp. Electron. Syst.*, vol. 51, no. 2, pp. 1029–1038, Apr. 2015.

[26] M. Bica, K.-W. Huang, U. Mitra, and V. Koivunen, "Opportunistic radar waveform design in joint radar and cellular communication systems," in *Proc. IEEE Global Commun. Conf. (GLOBECOM)*, Dec. 2014, pp. 1–7.

[27] M. Bica, K.-W. Huang, V. Koivunen, and U. Mitra, "Mutual information based radar waveform design for joint radar and cellular communication systems," in *Proc. IEEE Int. Conf. Acoust., Speech Signal Process. (ICASSP)*, Mar. 2016, pp. 3671–3675.

[28] T. Guo and R. Qiu, "OFDM waveform design compromising spectral nulling, side-lobe suppression and range resolution," in *Proc. IEEE Radar Conf.*, May 2014, pp. 1424–1429.

[29] C. B. Barneto, S. D. Liyanaarachchi, T. Riihonen, L. Anttila, and M. Valkama, "Multibeam design for joint communication and sensing in 5G new radio networks," in *Proc. IEEE Int. Conf. Commun. (ICC)*, Jun. 2020, pp. 1–6.

[30] C. B. Barneto, S. D. Liyanaarachchi, T. Riihonen, M. Heino, L. Anttila, and M. Valkama, "Beamforming and waveform optimization for OFDM-based joint communications and sensing at mm-waves," in *Proc. 54th Asilomar Conf. Signals, Syst., Comput.*, Nov. 2020, pp. 1–6.

[31] S. D. Liyanaarachchi, C. B. Barneto, T. Riihonen, and M. Valkama, "Joint OFDM waveform design for communications and sensing convergence," in *Proc. ICC - IEEE Int. Conf. Commun. (ICC)*, Jun. 2020, pp. 1–6.

[32] M. Bica and V. Koivunen, "Radar waveform optimization for target parameter estimation in cooperative radar-communications systems," *IEEE Trans. Aerosp. Electron. Syst.*, vol. 55, no. 5, pp. 2314–2326, Oct. 2019.

[33] C. Baquero Barneto *et al.*, "Full-duplex OFDM radar with LTE and 5G NR waveforms: Challenges, solutions, and measurements," *IEEE Trans. Microw. Theory Techn.*, vol. 67, no. 10, pp. 4042–4054, Oct. 2019.

[34] C. Sturm and W. Wiesbeck, "Waveform design and signal processing aspects for fusion of wireless communications and radar sensing," *Proc. IEEE*, vol. 99, no. 7, pp. 1236–1259, Jul. 2011.

[35] C. Sturm, T. Zwick, and W. Wiesbeck, "An OFDM system concept for joint radar and communications operations," in *Proc. IEEE 69th Veh. Technol. Conf. (VTC Spring)*, Apr. 2009.

[36] Y. Zeng, Y. Ma, and S. Sun, "Joint radar-communication with cyclic prefixed single carrier waveforms," *IEEE Trans. Veh. Technol.*, vol. 69, no. 4, pp. 4069–4079, Apr. 2020.

[37] Y. Rahmatallah and S. Mohan, "Peak-to-average power ratio reduction in OFDM systems: A survey and taxonomy," *IEEE Commun. Surveys Tuts.*, vol. 15, no. 4, pp. 1567–1592, Mar. 2013.

[38] C. B. Barneto, S. D. Liyanaarachchi, M. Heino, T. Riihonen, and M. Valkama, "Full duplex radio/radar technology: The enabler for advanced joint communication and sensing," *IEEE Wireless Commun.*, vol. 28, no. 1, pp. 82–88, Feb. 2021.

[39] T. Jiang and Y. Wu, "An overview: Peak-to-average power ratio reduction techniques for OFDM signals," *IEEE Trans. Broadcast.*, vol. 54, no. 2, pp. 257–268, Jun. 2008.

[40] T. Huang and T. Zhao, "Low PMEPR OFDM radar waveform design using the iterative least squares algorithm," *IEEE Signal Process. Lett.*, vol. 22, no. 11, pp. 1975–1979, Nov. 2015.

[41] *NR; Base Station (BS) Radio Transmission and Reception*, 3GPP document TS 38.104 v15.10.0, Tech. Spec. Group Radio Access Network, Rel. 15, Jul. 2020.

[42] S. M. Kay, *Fundamentals of Statistical Signal Processing: Estimation Theory*. Upper Saddle River, NJ, USA: Prentice-Hall, 1997.

[43] T. Zhao and T. Huang, "Cramer-Rao lower bounds for the joint delay-Doppler estimation of an extended target," *IEEE Trans. Signal Process.*, vol. 64, no. 6, pp. 1562–1573, Mar. 2016.

[44] S. Boyd and L. Vandenberghe, *Convex Optimization*. Cambridge, U.K.: Cambridge Univ. Press, 2004.

Sahan Damith Liyanaarachchi (Graduate Student Member, IEEE) received the B.Sc. degree (Hons.) from the University of Peradeniya, Sri Lanka, in 2016, and the M.Sc. degree (Hons.) from Tampere University, Finland, in 2019, where he is currently pursuing the Ph.D. degree with the Unit of Electrical Engineering. His research interests include waveform optimization for joint communication and sensing systems, with current research interest includes the evolution of beyond 5G systems.

Taneli Riihonen (Member, IEEE) received the D.Sc. degree (Hons.) in electrical engineering from Aalto University, Helsinki, Finland, in 2014. He is currently a tenure-track Assistant Professor with the Faculty of Information Technology and Communication Sciences, Tampere University, Finland. His research interests include physical-layer OFDM(A), multiantenna, multihop, and full-duplex wireless techniques with current research interest includes the evolution of beyond 5G systems.

Carlos Baquero Barneto (Graduate Student Member, IEEE) received the B.Sc. and M.Sc. degrees in telecommunication engineering from the Universidad Politécnica de Madrid, Spain, in 2017 and 2018, respectively. He is currently pursuing the Ph.D. degree with the Unit of Electrical Engineering, Tampere University, Finland. His research interests include joint communication and sensing systems' design, with particular emphasis on 5G and beyond mobile radio networks.

Mikko Valkama (Senior Member, IEEE) received the M.Sc. and D.Sc. degrees (both with Hons.) from the Tampere University of Technology in 2000 and 2001, respectively. He is currently a Full Professor and the Head of the Unit of Electrical Engineering, Tampere University. His research interests include radio communications, radio localization, and radio-based sensing, with particular emphasis on 5G and beyond mobile radio networks.